Title
Demonstration of a high repetition rate capillary discharge waveguide

Journal
Journal of Applied Physics, 119(3)

ISSN
0021-8979

Authors
Gonsalves, AJ
Liu, F
Bobrova, NA
et al.

Publication Date
2016-01-21

DOI
10.1063/1.4940121

Peer reviewed

Demonstration of a High Repetition Rate Capillary Discharge Waveguide

A. J. Gonsalves, C. Pieronek, J. Daniels, S. S. Bulanov, W. L. Waldron, D. E. Mittelberger, and W. P. Leemans,[1]
N. A. Bobrova,[2] P. V. Sasorov,[2] and F. Liu, S. Antipov, J. E. Butler[3]
[1)] *Lawrence Berkeley National Laboratory, Berkeley, CA 94720, USA*
[2)] *Keldysh Institute of Applied Mathematics, Moscow, Russia*
[3)] *Euclid TechLabs*

(Dated: 2 November 2015)

A hydrogen-filled capillary discharge waveguide operating at kHz repetition rates is presented for parameters relevant to laser plasma acceleration (LPA). The discharge current pulse was optimized for erosion mitigation with laser guiding experiments and MHD simulation. Heat flow simulations and measurements showed modest temperature rise at the capillary wall due to the average heat load at kHz repetition rates with water-cooled capillaries which is promising for applications of LPAs such as high average power radiation sources.

I. INTRODUCTION

The high acceleration gradient possible with laser-driven plasma accelerators[1] and recent progress such as the production of high-quality GeV electron beams[2–7] has increased interest in laser-plasma accelerator technology as a driver for radiation sources,[8–13] and as a path towards a TeV-class linear collider[14,15].

For both radiation source and high energy physics applications, repetition rates $\gtrsim$ kHz are required. As an example, compact LPAs offer the possibility of a portable system to actively interrogate targets which may contain special nuclear materials. The device would use Thomson scattering of laser light from the electron beam to produce a tunable high flux beam of gamma rays. Key to realizing this system is achieving the desired gamma ray photon flux and bandwidth (10^{10} to 10^{12} photons/second, $< 2\,\%$ energy spread)[16], which in turn requires increasing the repetition rate of high-energy LPAs from $\approx 1\,\mathrm{Hz}$ to $\gtrsim 1\,\mathrm{kHz}$.

For LPAs with higher repetition rate to be realized, femtosecond laser technology must be scaled to average power 100 times the current state-of-the-art and advances in fiber lasers and diode pump sources are motivating further research toward this goal[17]. The plasma source must also support kHz operation but capillary discharge waveguides (which have been shown to maximize electron beam energy for a given laser power[2,18]) currently operate at repetition rates of $\approx 1\,\mathrm{Hz}$[19]. This type of waveguide involves striking a discharge inside a capillary filled with low atomic number gas (usually hydrogen), where Ohmic heating of the plasma and heat conduction to the capillary wall give rise to a density profile with minimum on-axis that is suitable for guiding high-intensity laser pulses[20].

In addition to providing focusing forces for laser pulses in LPAs, capillary discharge waveguides have also been shown to be an effective focusing element for electron beams via the discharge current and associated magnetic field[21]. This provides a compact, tunable, and symmetric lens for transporting electron beams to targets and between independently powered LPA stages to achieve very high electron beam energy[22]. These waveguides have also been shown to be beneficial for high harmonic generation[23] and extreme ultraviolet lasing[24]. For all of these applications, increasing the repetition rate is important.

One potential limitation to the repetition rate of capillary waveguides is erosion of the wall material. Erosion can take place within a single discharge shot or be due to the high average power of multiple shots. Although less prone to erosion than other types of discharge waveguide[25–27], previous measurements at low ($\approx 1\,\mathrm{Hz}$) repetition rate showed that after 1.3×10^6 discharge shots the sapphire capillary wall had eroded up to a depth of $\approx 30\,\mu\mathrm{m}$[28]. This was for a square capillary of side $210\,\mu\mathrm{m}$ filled with 45 Torr of hydrogen and a current pulse with peak 300 A. Although this erosion is acceptable for 10 Hz systems, such erosion of the capillary wall is not compatible with long term operation at kHz repetition rates since the depth of the plasma channel depends on the radius of the capillary[20].

Mitigation of erosion of the capillary wall can be achieved by reducing the heat flux. The parameters that can affect this include current pulse width and amplitude, fill pressure, and capillary radius. The primary parameter for reducing heat flux is the current pulse amplitude since the rise time of the current pulse must be $\gtrsim 100\,\mathrm{ns}$ in order for the plasma channel to form[20], and typically one fixes the initial fill pressure and capillary radius to set the required density and plasma channel depth for the application. One method of determining the minimum current required to form a plasma channel is to perform laser-guiding experiments where both the laser energy transmitted through the waveguide and the size of the laser spatial mode at the exit of the capillary provide evidence for the formation of a plasma channel. Surface profile measurements were employed to determine whether erosion was taking place.

Using diamond instead of sapphire as the capillary wall material could also reduce the temperature at the capillary wall (single-shot or average) and mitigate erosion because of its high thermal conductivity at room temperature (up to five times that of copper and fifty times larger than sapphire). Other potential benefits result from various properties of diamond: compatibility with hydrogen based plasmas, chemical erosion resistance, thermal

shock resistance, negative electron affinity of the hydrogen terminated surface, optical and IR transparency. The potential increase in repetition rate afforded by diamond is investigated here using heat transfer simulations.

In this paper we determine the minimum amplitude of the current that is able to generate a plasma profile suitable for guiding, in order to reduce the heat deposition to the capillary walls. We demonstrate stable operation of the capillary discharge at 1 kHz repetition rate, and show that the effect of average temperature rise of the capillary wall material and gas can be mitigated by adjusting the gas flow. Operation for 10 million discharges showed no erosion within the 0.6 μm error.

The paper is organized as follows. Section II presents simulation and experiments resulting in the mitigation of erosion, including measurements of the plasma channel with guiding of femtosecond laser pulses and erosion of the capillary wall. Section III describes the limitations on repetition rate due to average power deposition and presents experiments demonstrating operation of the waveguide at a repetition rate of 1 kHz. Conclusions and prospects for a GeV-class laser plasma accelerator operating at repetition rates in excess of 1 kHz are discussed in Section IV.

II. MITIGATION OF SINGLE-SHOT EROSION

Minimizing the peak current of the discharge will reduce the peak temperature at the capillary wall and potentially avoid melting and erosion. In this section the minimum current required for waveguide formation is derived first from theory and simulation in Sec. II A, and then determined experimentally in Sec. II B

A. Theory and simulation of the minimum current required for waveguide formation

As described in Ref.[20] there are three stages of the plasma evolution in a hydrogen-filled capillary discharge waveguide. During the first stage the magnetic field penetrates the plasma, which is heated and ionized locally. Radial distributions of the plasma parameters remain homogeneous. As the electric current increases, the thermal conduction becomes significant at approximately the time of complete ionization of the plasma. During the second stage a redistribution of the plasma temperature and density across the channel occurs. In the third stage the discharge plasma is in dynamic and thermal quasi-equilibrium. A simple quasi-static model of the capillary discharge in the third stage (QSM)[20] predicts the plasma temperature and density using a balance between ohmic heating and cooling due to electron heat conduction to the capillary wall. During this phase the plasma pressure is almost uniform, and the electron density profile is approximately parabolic with a minimum on the axis, where the plasma temperature is maximum. Guiding of laser pulses is then possible due to the density profile that near the axis can be approximated by $n_{\rm e}(r) = n_{\rm e}(0) + br^2$[20]. A laser pulse with a Gaussian transverse profile will propagate through the waveguide with a constant intensity profile if the spot size ($1/e^2$ radius of intensity profile) $w_0 = W_{\rm M} \equiv (\pi r_{\rm e} b)^{-1/4}$[29], where $r_{\rm e}$ is the classical electron radius.

An estimate of the current required for waveguide formation can be made by assuming that the on-axis temperature must exceed the temperature required for full ionization of the hydrogen. The temperature on the axis of the capillary can be estimated using the QSM by[20]:

$$T_{\rm e}({\rm eV}) = 5.7 \left[\frac{I({\rm kA})}{r_{\rm cap}({\rm mm})} \right]^{2/5}, \qquad (1)$$

where $T_{\rm e}$(eV) is the electron temperature, I(kA) is the current flowing through the plasma, and $r_{\rm cap}$(mm) is the radius of the capillary. A temperature of approximately 3 eV is required for full ionization, requiring a peak current of 25 A for $r_{\rm cap} = 125$ μm. This estimate does not include the temporal evolution of the plasma, and that for higher density and shorter current pulses, sufficient energy may not be deposited to reach the quasi-static state. In order to predict the minimum current required for typical current pulses with a rise time of ≈ 100 ns, magnetohydrodynamic (MHD) simulations were performed.

Spatial and time dependences of plasma electron density and temperature in capillary discharge were evaluated by means of one-dimensional two-temperature (ion and electron) one-fluid MHD code. For the capillary discharge under consideration, the quasi-static state is determined mainly by electron thermal conductivity and Joule heating. It is also necessary to incorporate the degree of ionization both into the equation of state and into the dissipative coefficients.

Since the length of the capillary is much larger than its diameter, it is reasonable to use the one-dimensional approximation. The set of dissipative MHD equations used here was described in[30–32]. The expressions for the dissipative coefficients and the rate of the thermal transfer between ions and electrons were taken from[33], where the possible considerable difference between the Coulomb logarithms λ_{ee}, λ_{ii} and λ_{ei} for electron–electron, ion–ion and electron–ion collisions, respectively, was taken into account. At low temperatures, as long as the mean ion charge is considerably less than unity, there is a fraction of neutral particles in the plasma. To take into account the partial ionization of hydrogen plasma we re-normalize the electron-ion collision frequency ν_{ei} by taking into account the contribution of neutral particles to the electron scattering. We assume that the conditions for the local thermodynamic equilibrium are satisfied separately for the electron and ion components. The local equilibrium state of ionization, z, corresponds to the minimum free energy at given T_e, T_i and specific volume of the atomic cell V. This equation generalizes the Saha equation for a plasma composed of atoms and singly-ionized ions to the case when $T_i \neq T_e$. In the case of the H-filled capillary

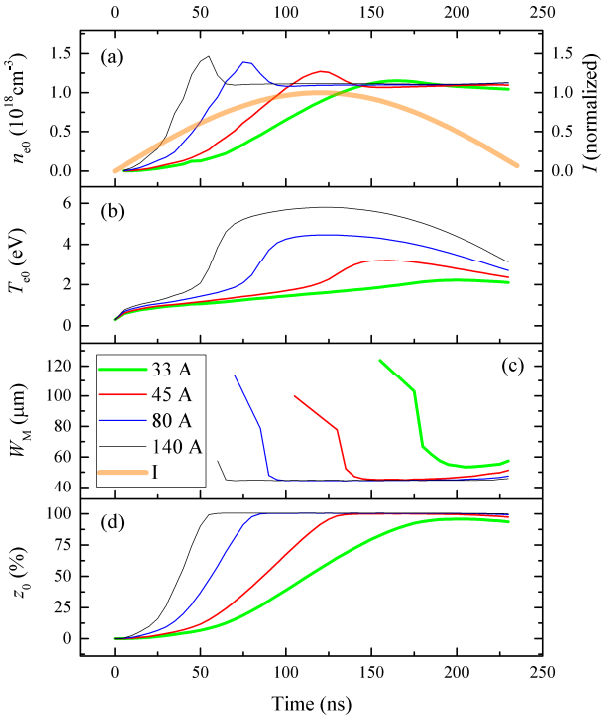

FIG. 1. The temporal evolution of the waveguide for electric currents of 140A, 80 A, 45A and 33A. The on-axis values of electron density, temperature, matched spot size, and ionization degree are shown in (a), (b), (c), and (d), respectively. Also shown in (a) is the normalized discharge current. For each value of current except for 33A, a stable density profile is observed for tens of ns [(a) and (c)], along with temperature on-axis above 3eV (which yields full on-axis ionization). Only the case of 33A does not provide plasma properties suitable for guiding. The plasma channel density and depth at $t = 150$ ns do not vary significantly with peak current.

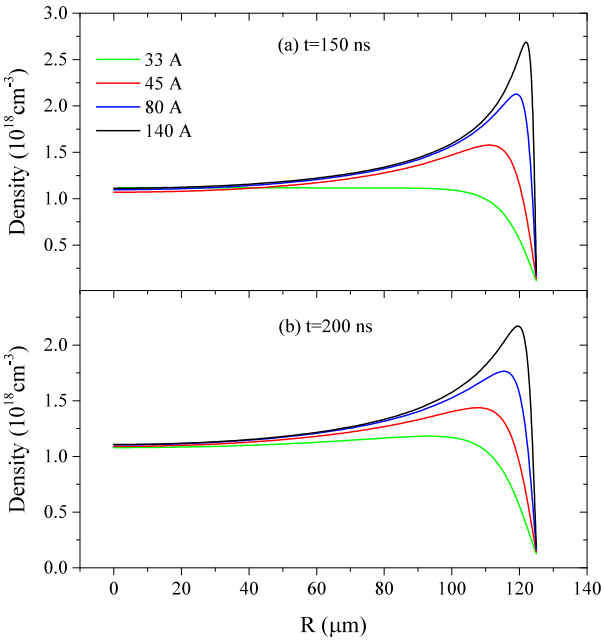

FIG. 2. The radial distributions of electron density at (a) 150 ns and (b) 200 ns for peak electric currents of 140A, 80 A, 45A and 33A. At t=150 ns a parabolic profile near the axis is observed for each current except for 33A, which shows a maximum on axis. For t=200 ns, the lowest-current case does show a minimum on-axis. However since the plasma on-axis is not fully ionized [see Fig. 1(d)], ionization-induced defocusing could adversely affect guiding.

discharge, the influence of radiation cooling on plasma dynamics is negligibly small because the magnitude of the electric current is significantly less than the Pease–Braginskii current value[34,35].

Initially there is no electric current inside the channel, and hence in order to initiate the discharge in the simulations, the gas was artificially pre-ionized by setting its initial temperature to 0.3 eV. We do not simulate the initial breakdown of the neutral hydrogen gas because, the duration of breakdown is short compared to the times of interest for formation of the plasma channel, and the details of the breakdown do not affect substantially the deduced properties of the plasma at later times. After the breakdown, the current pulse heats the plasma and creates an azimuthal component of the magnetic field.

There is no pinching of the plasma since the plasma pressure is considerably higher than the magnetic field pressure. The plasma is confined from expansion in the radial direction by the elasticity and the inertia of the capillary walls.

We use the physical model described above to simulate the discharge under the conditions of the experiment. In these simulations the capillary was taken to be made from sapphire with $r_{\rm cap} = 125$ μm and pre-filled with pure hydrogen of uniform density and temperature at an initial density of 2.9×10^{-6} g/cm^3, which corresponds to a pressure of 26 Torr at room temperature. For $t \geq 0$ the current was assumed to be of the form $I(t) = I_p \sin(\pi t/t_0)$, where $I_p = 140$ A, 80 A, 33 A and $t_0 = 120$ ns.

The results of the simulations are shown in Fig. 1, in which the three stages of plasma evolution are evident. The on-axis values for density, temperature, matched spot size, and ionization level are shown in (a), (b), (c), and (d), respectively. The matched spot size was calculated by performing a parabolic fit to $n_{\rm e}(r)$ over the range $r < 44$ μm. During the first stage the electric field penetrates the plasma very quickly (the skin time is on the order of 1 ns). Plasma is heated and ionized and, as the electric current increases, n_e, T_e, and z grow with time. Taking the example of $I_p = 140$ A this phase ends at ≈ 50 ns as the ionization level becomes high. During the second stage when less energy is required for ionization, the rate of rise in temperature increases rapidly. Thermal conduction to the wall becomes significant, causing the temperature profile to become peaked at the axis. In order to keep pressure constant across the the capillary, the plasma density reduces on-axis, as shown in Fig. 1(a) at 50 ns $< t <$ 60 ns for 140A.

During the third stage of the discharge the plasma is

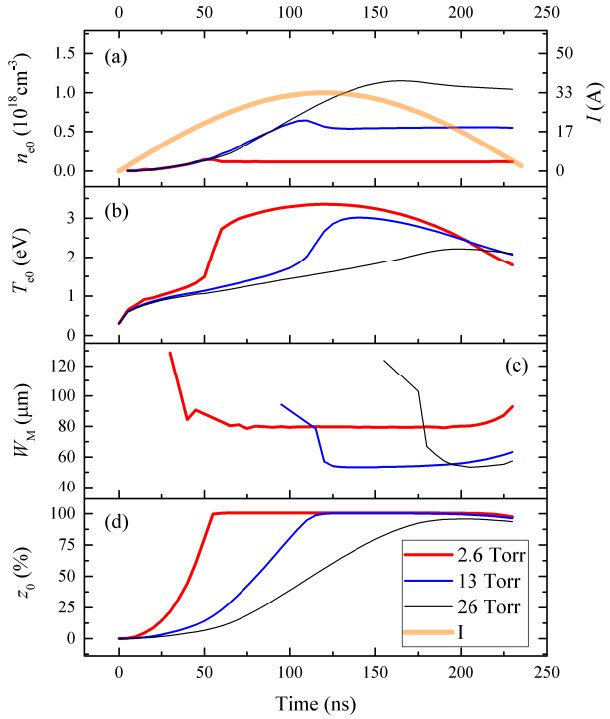

FIG. 3. The temporal evolution of the waveguide for three initial pressures: 26, 13, and 2.6 Torr. The on-axis density, temperature, matched spot size, and ionization degree are shown in (a), (b), (c), and (d), respectively. The discharge current is shown on each graph by squares (right axis). For $P_{\rm cap} = 26$ Torr and $I_{\rm p} = 33$ A full ionization on-axis is not achieved, but decreasing the density lowers the energy used for ionization and leads to higher temperature and stable plasma channels suitable for guiding.

in quasi steady-state equilibrium at a given electric current. The plasma pressure is almost homogeneous. The plasma temperature has its maximum on the axis, due to the fact that the Ohmic heating is balanced mainly by thermal conduction to the relatively cold capillary wall. Since the hydrogen is ionized to a high degree and at constant pressure, a monotonic radially-decreasing temperature results in an axial minimum in the electron density profile of the plasma. The on-axis temperature rises and falls with the instantaneous value of current. During this stage the plasma density profile varies only weakly with current (time), as shown by the on-axis density in Fig. 1(a) and the matched spot size in Fig. 1(c). This suggests that lower current can be used to achieve the desired density profile. Indeed for lower peak current (80 A and 45A) we see that the third stage (in which guiding of intense laser pulses is possible) is still reached, although it occurs for later times ($t \approx 100$ ns for $I_0 = 80$A, after $t \approx 140$ ns for $I_0 = 45$A). For 33 A the steady-state equilibrium is not established during the time of discharge, although a density-minimum on-axis is observed for some delays. The radial distributions of electron density at 150 ns for electric currents of 140A, 80 A, 45A and 33A are plotted in Fig. 2(a). An axial minimum in the radial electron density profile is well established for electric currents of 140A, 80 A and 45A, but not for 33A. Fig. 2(b) shows the density profiles at 200 ns. Although there is a density minimum on axis for all values of peak current, poor-quality guiding of intense laser pulses may be observed for the 33 A case because the partially ionized plasma [as shown in Fig. 1(a)] may result in ionization-induced defocusing of the laser pulse. For the 33 A case the maximum ionization degree of $\approx 96\,\%$ is achieved ≈ 80 ns after the peak of current. This corresponds to a potential increase in the on-axis density of 0.04×10^{18} cm^{-3}, which is approximately the same as the plasma channel depth at a radius of $W_{\rm M} = 54\,\mu$m. This will give rise to ionization-induced defocusing of spatially Gaussian laser pulses (but may be of interest for guiding of pulses with different spatial profiles[36]). In addition to the issue of ionization defocusing and formation of a weaker channel, operation close to threshold may result in loss of guiding profile at the cooler parts of the capillary (e.g. near gas entrance holes) which is not taken into account in this 1D treatment.

The simulations show that for initial gas pressure of 26 Torr, $I_p = 33$A is not enough to establish necessary conditions for channeling of laser pulses (although it should be noted that this may not be the case for a longer current pulse). We have also investigated the dependence on initial density (pressure). In Fig. 3 the dependence of axis density (solid line) and axis degree of ionization (dashed line) are shown for three initial pressures: 26, 13, and 2.6 Torr. The axial electron density is constant after $t \approx 60$ ns for 2.6 Torr, and after $t \approx 125$ ns for 13 Torr. Full ionization on the axis is achieved at $t \approx 50$ ns for 2.6 Torr, and at $t \approx 125$ ns for 13 Torr. This is expected from considerations of the energy required for ionization and shows that the peak current can be lowered for lower density.

B. Experimental determination of minimum current for waveguide formation

1. Experiment setup

The hydrogen-filled capillary discharge waveguide has been described in detail elsewhere[19,37–39]. For the experiments presented here the capillary was formed out of semi-circular grooves in two sapphire blocks of dimensions $4 \times 20 \times 33$ mm. The capillary had diameter $250\,\mu$m $\pm\, 5\,\mu$m and length 33 mm. The capillary was filled via 15 mm $-$ *long*, 500 μm-diameter gas inlets located 2 mm from each end to an initial pressure between the slots of 26 Torr unless otherwise stated. The gas inlets were in turn fed from meter-long plastic tubes of diameter 2.5 mm. The minimum expected matched spot size from the MHD simulations shown in Fig. 1 was 44.5 μm. The peak current was varied both by changing the charge voltage on the high voltage pulsed power supply capac-

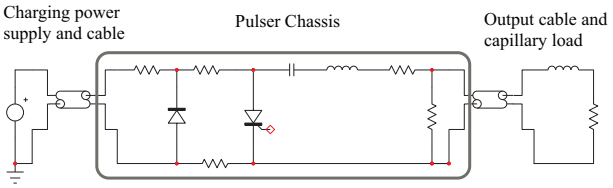

FIG. 4. Schematic of the pulsed power supply with the thyratron represented by a thyristor. The load is depicted as an output cable, stray inductance, and a resistor to represent the capillary discharge.

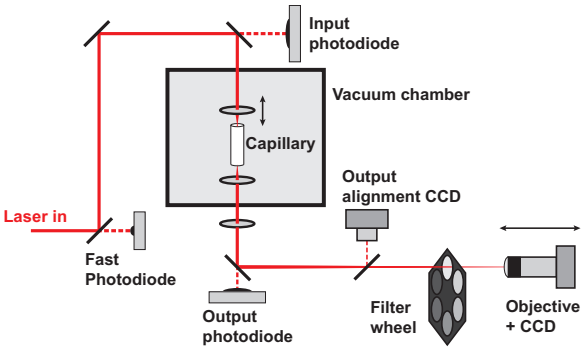

FIG. 5. The setup used to diagnose plasma channel formation in the capillary.

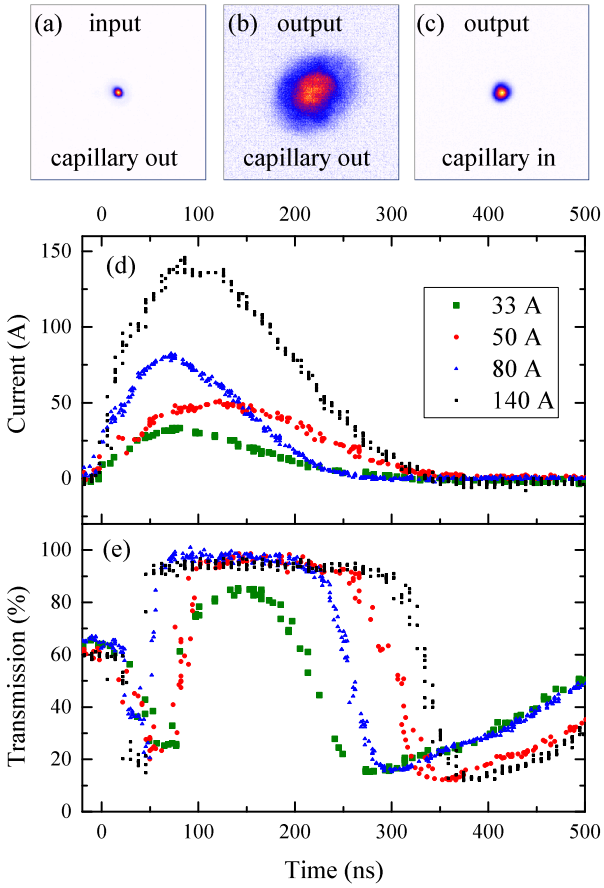

FIG. 6. The results of guiding laser pulses through the capillary. The mode input to the capillary, at the output plane of the capillary with capillary removed, and a typical guided mode are shown in (a), (b), and (c), respectively. Discharge current oscilloscope traces for the different high voltage pulsed power supply configurations are shown in (d). The percentage of laser energy transmitted through the capillary is shown in (e) as a function of delay for the configurations in (d). The systematic error in the determination of the energy transmission is estimated to be 5 %.

itors and the resistance and capacitance of the circuit shown in Fig. 4. Typical discharge current traces for the various configurations are shown in Fig. 6(d), with rise-times of ≈ 100 ns.

In order to experimentally determine the minimum current required for waveguide formation, guiding of femtosecond laser pulses was performed. The experiment setup (shown in Fig. 5) employs pulses from a Ti:sapphire regenerative amplifier, producing laser pulses of duration 40 fs, wavelength 800 nm, and bandwidth 30 nm. Pulses of energy 1 μJ were focused to a spot size of 38 μm (radius at which intensity drops to $1/e^2$ of the peak value) at the entrance of a hydrogen-filled capillary discharge waveguide. The energy and spatial mode of pulses transmitted through the capillary were measured with a photodiode and CCD camera, respectively. The current through the capillary was measured with a current transformer and oscilloscope. The relative delay between the laser pulse and the discharge current was measured with a photodiode and oscilloscope. Control over the input spot size was achieved with a telescope and beam energy with a waveplate and polarizer. For vacuum propagation, the laser mode at focus is shown in Fig. 6(a), and at the capillary exit plane in Fig. 6(b). An example of a mode exiting the capillary for peak current of 50A is shown in Fig. 6(c).

2. Results on the minimum discharge current required

The portion of the energy transmitted through the waveguide is plotted as a function of delay in Fig. 6(e). For 50, 80, and 140 A the peak energy transmission is above 90 % for $t \gtrsim 100$ ns. For peak current 33 A it can be seen that the peak transmitted laser energy and width of high transmission drops significantly. Given the timing jitter of $\lesssim 10$ ns, current pulses with peak current 50 A and above are deemed suitable for guiding. This is for current pulse full-width-half-maximum $\tau_I(\mathrm{FWHM}) \approx 160$ ns, density $n_e \approx 10^{18}\,\mathrm{cm}^{-3}$ and capillary radius $r_{\mathrm{cap}} = 125\,\mu\mathrm{m}$. This is consistent with the MHD simulations presented in Fig. 1.

C. Wall erosion measurements at low repetition rate

Erosion measurements in this section were performed measuring the surface of capillaries before and after firing a large number of discharges at a repetition rate of a few Hz. Two measurement techniques were employed. The first technique was performed on trapezoidal capillaries where one side was initially optically polished. The channel dimensions were chosen to approximate the cross-sectional area of a 250 µm-diameter circular capillary. The extent of wall erosion by the plasma was determined by comparing microscope images of the optical surface, as well as the capillary ends. Erosion would manifest as pitting of the optical surface as well as the enlargement of the capillary ends.

For a 168 µm-wide (average), 208 µm-deep, 33 mm-long capillary filled with 26 Torr neutral hydrogen, which was exposed to 5×10^4 discharges with a current pulse peak of 160 A and FWHM 150 ns, pitting of the optical wall and enlargement of the ends was visible in the microscope images, indicating that erosion was taking place for these conditions. For a 230 µm-wide (average), 244 µm-deep, 33 mm-long capillary filled with 26 Torr neutral hydrogen, which was exposed to 5×10^5 discharges with a current pulse peak of 80 A and FWHM 125 ns, no modification to the optical surface was observed.

For a more precise comparison with the guiding data, erosion was also measured in the capillary with circular cross-section using an interferometric surface profiler. These measurements also allow for determination of whether the rougher surface of the circular capillaries has an effect on erosion. For the case of 80 A, the surface profile of the capillary was measured before and after 5×10^5 discharges with initial pressure 26 Torr. To within the 0.6 µm error in the measurement, no erosion was observed. If we assume that an application can tolerate a 10 % change in matched spot size and that the erosion per shot is constant, we can use the inverse square root dependence of matched spot size with radius derived in Ref.[20] to estimate that the capillary can be operated for at least an hour at a repetition rate of 1 kHz. In order to show that the capillary can be operated for longer periods in reasonable time, a more accurate measurement of eroded volume or higher repetition rate discharge is required. The next section describes the development of a capillary discharge waveguide operating at 1 kHz, which allowed for better determination of the potential erosion rate.

III. DEMONSTRATION OF KHZ OPERATION

A. Average Power Limitations

If the average power dissipated into the capillary wall becomes too high, melting will occur. To determine this limitation on repetition rate in this section we report on steady-state solutions of the heat dissipation in sapphire and diamond capillary waveguides. The model used treats the thermal parameters of the materials as functions of temperature. Conductive heat transfer is governed by:

$$\mathbf{q} = -k(T)\,\nabla T, \tag{2}$$

where $\mathbf{q}$, $k(T)$ and T are the heat flux, thermal conductivity and temperature, respectively. The heat transfer equation was solved subject to the boundary conditions, which are constant heat flux at the inner capillary wall and constant temperature of 300 K (corresponding to room temperature water cooling) at the outer surface.

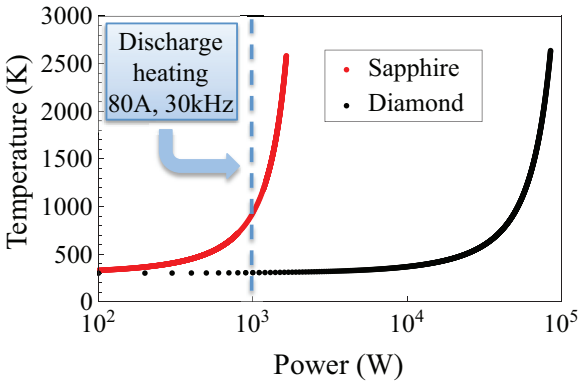

FIG. 7. Shown in (a) is the wall temperature as a function of power dissipated in a cylindrical capillary of radius 125 µm, outer diameter 2 mm, and length 33 mm obtained by solving Eq. 2 for sapphire (red) and diamond (black).

Figure 7 shows the maximum temperature as a function of power dissipated in a sapphire and diamond cylindrical capillary of radius 125 µm, outer diameter 2 mm, and length 25 mm. Considering the melting point of sapphire (≈ 2300 K) vs diamond (≈ 3800 K), the power that can be tolerated is two orders of magnitude higher for diamond than for sapphire.

To place limits on repetition rate we first estimate the energy deposited into the capillary per shot. For example the Spitzer resistivity calculated from the temperature and density for the 80 A case of Fig. 1 yields an energy deposited into the structure of ≈ 30 mJ using Ohms law. Taking the example of 1 kW from Figure 7(a) where the temperature is still well below that of the melting point for sapphire, the maximum repetition rate for the 80 A case is ≈ 30 kHz.

B. Repetition Rate Limitation due to Capillary Refill Time

The time required to refill the capillary after a discharge can also limit the repetition rate. After a discharge is struck the plasma temperature and pressure rise in ≈ 100 ns. The plasma will expand rapidly into the vacuum region and the gas feed slots and cool until pressure of the hot gas matches the upstream feed gas pressure (in a few tens of µs).

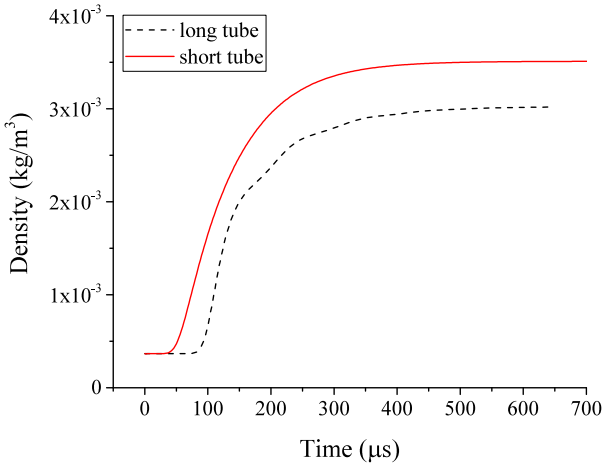

FIG. 8. Temporal evolution of the density in the middle of the capillary that is re-filled after a discharge shot.

In order to place an upper limit on this expansion, the peak radially-averaged temperature and density inside the capillary were taken from the the 80 A, 26 Torr MHD simulation. Assuming adiabatic expansion into the gas slots alone (which will overestimate the expansion) it is estimated that the hot gas expands a few mm inside the 2.5 mm-diameter plastic tubing, and the temperature is a few thousand kelvin.

Time-resolved 3D simulations to determine the refilling time after the expansion phase were run using the FLUENT computational fluid dynamics package in ANSYS 14.5[40]. Laminar flow was assumed with the slip boundary formulation for low-pressure gas systems, which extends the laminar flow model into the transition regime.

The gas feed slots and capillary were fed by a reservoir of hydrogen with a volume orders of magnitude larger. The capillary length and diameter were 33 mm and 250 μm, respectively. Two cases were investigated bracketing the estimated expansion, the first of which had gas feed geometry matching the experiment and an expansion 30 mm into the plastic tubing. The second was for a modified geometry where the gas slots in the sapphire were 3 mm-long and directly attached to the constant-pressure reservoir.

The reservoir and all tubes were initially filled with 34 Torr hydrogen. The reservoir was initialized with 300 K and the tubes with 3000 K. The exit of the capillary emptied into a vacuum region with a fixed 100 mTorr static pressure at its boundary. The system was allowed to evolve in 100 ns steps for 600 μs via a coupled pressure-velocity solution scheme with second order spatial discretization.

The results are shown in Fig. 8, which shows the density in the middle of the capillary as a function of time. For both cases the capillary refills in less than 1 ms, which supports 1 kHz operation. For the first case with longer fill tube and geometry that matches the experiment, after 600 μs, the capillary had refilled with pressure variation less than 0.2 % between the gas slot and the capillary center. The equilibrium flow rate was 6.3×10^{-8} kg/s. The measured flow rate was 6.4×10^{-8} kg/s. The simulated pressure inside the capillary was 27.5 Torr compared with the measured value of 26 Torr, the small difference likely due to the fact that the simulation does not include the almost meter-long plastic tubing to the upstream pressure meter.

The results show that the capillary refills on sub-ms timescales, and that the refill time is dominated by the time to fill the capillary section, allowing for kHz repetition rates with the current design. Shorter capillaries or additional gas feeds could be used to decrease refill time further.

C. The 1 kHz pulsed power supply

Since the gas refill time is sub-ms, a pulsed power supply capable of kHz repetition rates was built. The design (described in detail in Ref.[41]) was kept similar to the 1 Hz pulsed power supply used for the guiding experiments presented here and in previous experiments[19,37,38], employing a damped RLC discharge circuit where the energy storage capacitor and lumped element wave-shaping and current-limiting components can be easily adjusted to accommodate a range of capillary discharge requirements.

The charging system is based on a conventional 8 kJ/s capacitor charging supply (TDK-Lambda 802L). There is also a conventional resistor network and diode string in the pulser chassis to protect the power supply from voltage reversal and to protect the switch from the stored energy in the power supply cable (see Fig. 4). At 1 kHz the average power dissipated in series resistors and the switch from the cable capacitance is ≈ 100 W. Forced air cooling is used for the series resistor array and the switch.

D. Demonstration of kHz operation

In this section the operation of a capillary at kHz repetition rates is demonstrated. As shown in Section III A, it was expected that operation at kHz repetition rate causes approximately 30W to be deposited into the capillary wall. Since the capillary is in vacuum and has poor thermal contact with the chamber, it was necessary to add external cooling. A water-cooled version of the waveguide was built. Water at 22 °C was flowed across one of the two sapphire blocks (the surface opposite the semi-cylindrical groove) using a closed loop chiller system with 230 W cooling capacity.

In order to determine if the plasma is affected by operation at high repetition rates, several diagnostics were employed. The optical emission from the plasma was

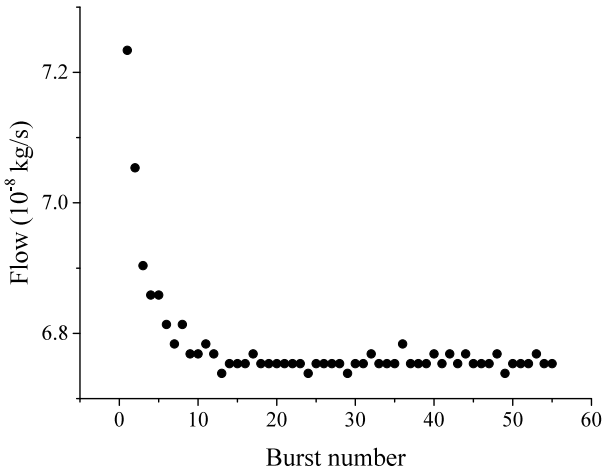

FIG. 9. Flow rate vs burst number for 1 kHz repetition rate and pressure 28 Torr. Each burst was 5 s-long and the time between the end of a burst and the beginning of the next was 5 s.

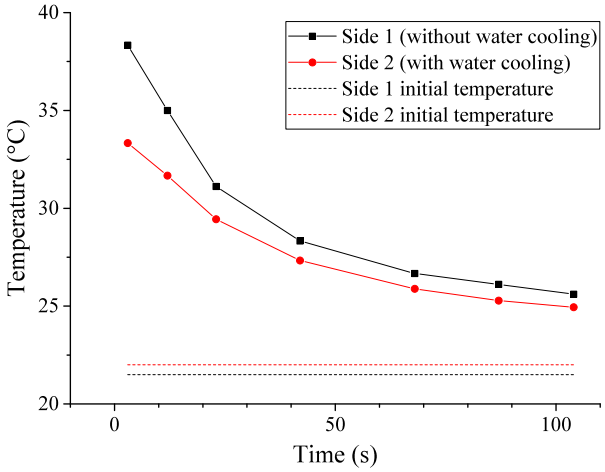

FIG. 10. After 15 minutes 1 kHz discharge at 70 A and 32 Torr hydrogen in capillary, the temperatures decay behavior read by copper thermocouple on both sides of the sapphire capillary.

measured using a time-averaged spectrometer and photodiode, and the mass flow rate of hydrogen measured at the entrance to the vacuum chamber using a pressure controller with built-in flow meter. At 1 kHz repetition rate both the optical plasma emission and flow rate were reduced compared to 1 Hz case. Fig. 9 shows the flow measured immediately before bursts of 1000 discharges separated by 1 ms. The time between the end of a burst and the beginning of the next was 5 s, which is longer than the time required to refill the capillary after a discharge is fired. This is confirmed experimentally by the fact that at 1 Hz repetition rate the flow and light yield are constant. The average repetition rate was 500 Hz. It can be seen that the flow rate reduces but stabilizes after about 15 bursts (150 s). Since the pressure inside the capillary is measured by the sensor lines directly coupled to the capillary and held constant, a rise in temperature of the gas and associated reduction in density is the likely cause of decrease in reduced light yield and flow.

In order to quantitatively determine if the gas temperature explanation for reduced flow is plausible, we model the flow. Typically computationally-expensive direct simulation Monte Carlo (DSMC) methods or slip-corrected fluid models are used since the flow transitions to rarefied flow close to the capillary ends. Here we leverage the analytic framework developed in Ref.[42], where the mass flow rate through a tube of length l with a pressure drop ΔP is given by

$$\dot{M} = \frac{G\pi r_{\rm cap}^3 \Delta P}{l}\left(\frac{m}{2kT}\right)^{1/2}, \qquad (3)$$

where m is the molecular mass of the gas, k is the Boltzmann constant, and T is the temperature of the gas. The dimensionless flow rate G can be calculated using

$$G = \delta_a/4 + 1.0162 + 0.5489/\delta_a - 0.6081/\delta_a^2, \qquad (4)$$

where δ_a is the average of the rarefaction parameters at the entrance and exit of the tube. The rarefaction parameter is defined by $\delta = \sqrt{\pi} r_{\rm cap}/2\lambda$, where λ is the mean free path. The flow calculated from Eq. 3 using $T = 295$ K is 7.8×10^{-8}kg/s. For the flow measured before the first burst, the flow was 7.2×10^{-8}kg/s, which agrees with the calculated flow to well within the 20 % error in the flow measurement. In order to match the experimentally measured percentage drop in flow from the first burst to the stabilized value in Fig. 9 the model requires an increase in temperature of ≈ 20 K.

In order to determine if the temperature rise of the gas calculated from the reduction of flow during kHz operation is reasonable, thermocouple measurements were undertaken using type K thermocouples that had time to reach 99 % of actual value almost 1 minute. Thermocouples were placed on the outer walls of the capillary (4 mm from the capillary axis). The temperature rise of 33 mm-long 250 µm-diameter capillary was measured after a kHz discharge test that ran continuously for 15 minutes (0.9 million shots) with peak current of 70 A and 32 Torr hydrogen in capillary. Since electrical noise due to the discharge prevented measurement during kHz operation, measurement using the handheld thermocouple reader could only begin several seconds after the discharge burst had stopped. Before the discharge was struck the temperature measured on the water-cooled side was 21.7 °C and 22.2 °C on the other side.

The temperature as a function of time after the discharge burst is shown in Fig. 10. The temperature rise at the outer wall is $\approx$ 20 K. The complicated geometry would require simulation to determine the precise temperature at different locations in the capillary and

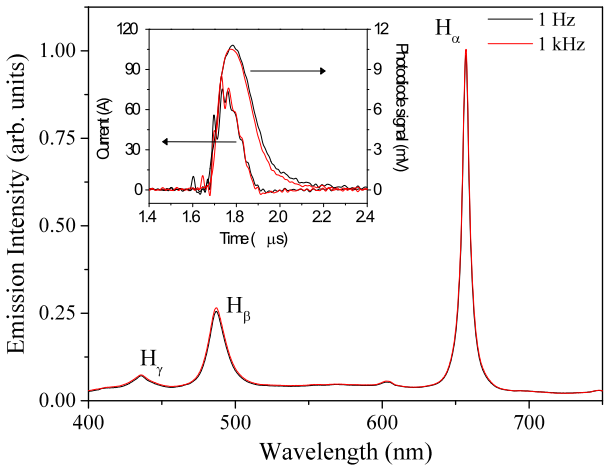

FIG. 11. Emission spectra for repetition rate 1Hz (black) and 1 kHz (red) for peak current 80 A in a capillary of radius 125 μm. For the 1Hz data the initial fill pressure was 30 Torr. For the 1 kHz data the flow rate was increased by 25% to compensate for reduced density.

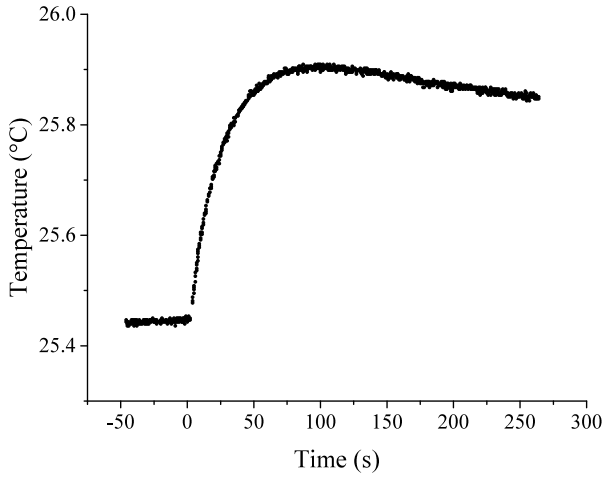

FIG. 12. Temperature rise measured on the outer wall of the capillary after 1000 discharges at 1kHz for charge voltage 17.4 kV, peak current 80 A, and initial hydrogen fill pressure 26 Torr.

gas slots but this is in reasonable agreement with the the ≈ 20 K rise calculated from half-duty-cycle data of Fig. 9. The reduced average repetition rate will reduce the measured temperature but the temperature rise at the capillary-gas interface will be larger than that measured on the outer wall of the capillary. The results should therefore be considered simply as a demonstration of the effect of gas temperature increase.

If for higher repetition rate the gas temperature increases and the molecular density decreases, an increased flow rate is required to achieve the same plasma conditions as the low repetition rate case. The time-averaged spectrum and photodiode signals of single discharges were used to demonstrate this. Note that if the density was changed, the linewidth of the hydrogen lines would change as well as the overall light intensity, and if the temperature was altered the hydrogen line to continuum ratios would be different. Fig. 11 shows spectra and photodiode signals at 1Hz and 1 kHz discharge modes at same voltage but flow of the kHz case adjusted to equal the light yield of the 1Hz case. The results on the two repetition rates for both diagnostics match well, suggesting the plasma is not affected by operation at kHz repetition rates (as long as the molecular density is kept constant by adjusting the flow). The stability of the plasma was improved for the 1 kHz case, as measured by an improvement in the standard deviations in integrated discharge current from 4.5 % to 1.8 %, and in light yield from 4.3 % to 1.6 %. This may be due heating of the electrodes or the thyratron switch.

For further comparison with MHD simulation the energy deposited into the sapphire per shot was measured. Since precise simulation of the geometry would be required to retrieve this from the data in Fig. 10, it was decided to measure the temperature rise of the sapphire blocks where heat loss was small and could be taken into account. Three changes to the thermocouple measurements allowed for this. First, the water cooling system was disconnected to reduce heat conduction from the sapphire. Second, the thermocouple was read via computer so that the temporal evolution of the temperature could be measured on a faster timescale. And finally, short (1 second) kHz bursts were used to deposit a finite amount of energy into the sapphire. An example measurement of a single burst taken in a 33 mm-long 250 μm-diameter capillary is shown in Fig. 12. The gap in the temperature measurement is due to electrical noise from the discharge. It was not possible to measure the temperature during the discharges but since the timescale for heat equilibration in sapphire blocks of the size employed is more than 1 second and time for reaching equilibration value about a minute, data during this time is not required.

Using the size of the sapphire blocks and the specific heat capacity of sapphire, and extrapolating to take into account the slow response of the thermocouple, the heat deposited into the sapphire can be calculated. The results of this calculation are shown in Fig. 13, which shows the heat deposited as a function of peak current. Also shown is the heat deposited to the plasma as calculated from MHD simulations. The simulated temperature was used to calculate the Spitzer resistivity and the power vs time curve was integrated to get the total heat deposited. The MHD result measures the total heat deposited to the plasma and does not take into account energy lost through plasma and hot gas ejection which continue to occur after the discharge current has ceased. Three-dimensional MHD simulations (or an estimate of the expansion of the plasma and subsequent gas along with transfer of heat to the walls) would be required for a more precise comparison with experiment. The current results are however sufficient for validating the

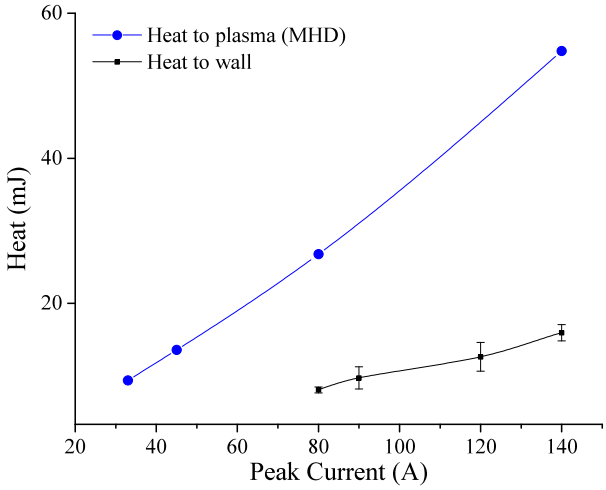

FIG. 13. Heat deposited per discharge in a capillary of diameter 250 µm filled with hydrogen at 26 Torr as a function of discharge voltage. The black squares are calculated from temperature rise measurements after 1second-long kHz bursts and the blue circles are the result of a Spitzer resistance calculation of MHD data. The MHD result measures the total heat deposited to the plasma and does not take into account energy lost through plasma and hot gas ejection which continue to occur after the discharge current has ceased.

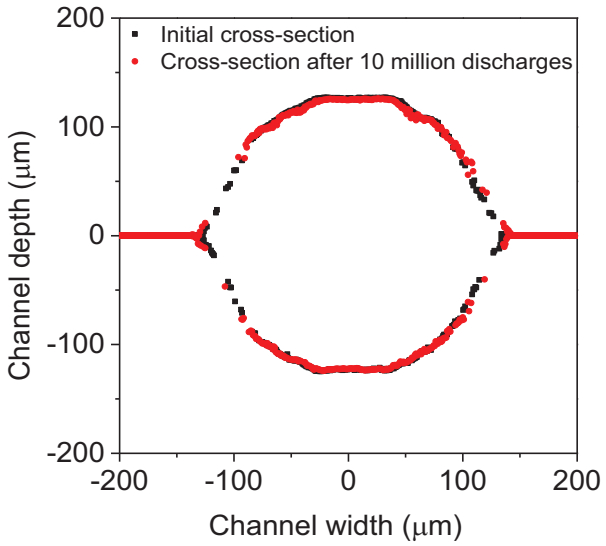

FIG. 14. Measured profiles averaged over a 10 µm-long section at the center of the capillary before and after 10 million shots for: peak current of 80 A; initial hydrogen fill pressure of 26 Torr; and repetition rate of 1 kHz.

discussion on maximum repetition rate afforded by the sapphire capillary.

E. Erosion measurements at kHz repetition rate

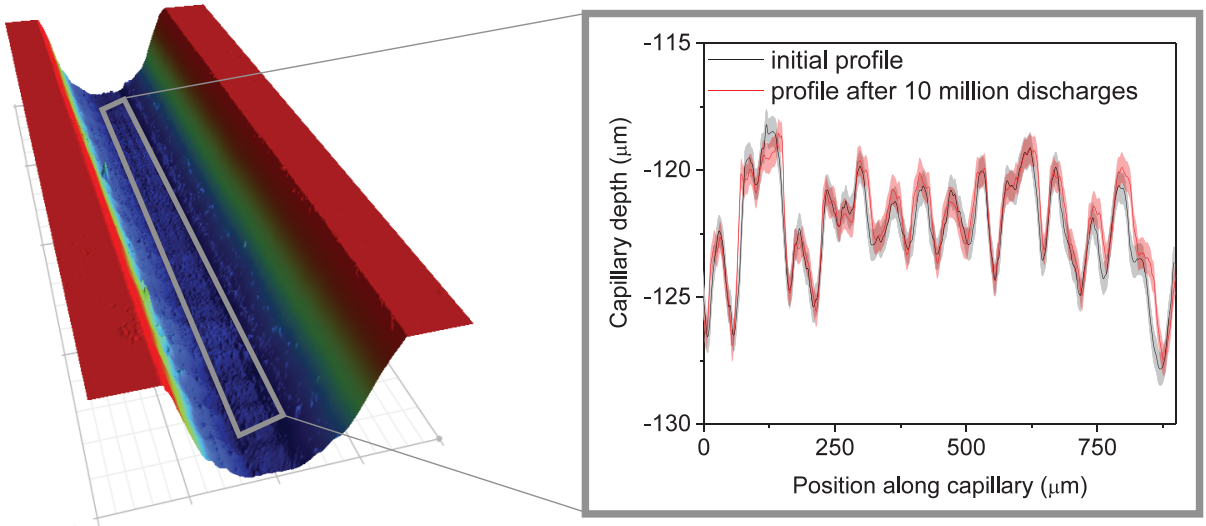

FIG. 15. Left: example surface profile measurement corresponding to a 1 × 0.43 mm area consisting of auto-stitched 0.58 × 0.43 mm images. The measurement is centered on the 33mm-long capillary in the direction of the capillary axis. The grey box represents the 1 mm × 35 µm area that was used to produce the graph on the right, which shows profiles along the capillary axis averaged over the central 35 µm.

In order to determine the feasibility for long-term kHz operation, the water-cooled sapphire capillary (length 33 mm and diameter 250 µm) was exposed to 10 million discharges at 1 kHz repetition rate. The peak current

was 80 A and the hydrogen pressure inside the capillary was 26 Torr.

The surface profiles of the two semi-circular channels measured with an interferometric profiler before and after the discharges are shown in Fig. 14. The data corresponds to an average over 10 μm in the center of the capillary.

It can be seen from Fig. 14 that shape and size of the capillary did not change significantly. To examine this with greater accuracy the surface profiles along the capillary axis averaged over a central width of 35 μm are shown in Fig. 15. The black line shows the initial profile and the red the profile after exposure to 10 million discharge shots. The shaded areas correspond to the rms error as calculated from separate measurements on an 8 μm VLSI/NVLAP step height standard which yielded 0.5 % error. For the capillary measurements in the center of the channel this corresponds to an error of 0.6 μm. The actual error on an individual pixel may be slightly higher. The few micron variations seen in the initial profile are due to the laser machining process. These laser-machining artifacts before and after the erosion test are well within the error for the majority of the measurement. Taking the mean of these profiles, the initial and post-experiment depths were 122.5, and 122.1 μm, respectively. Thus no erosion was observed within the 0.6 μm error after 10 million shots, corresponding to 2 hours and 45 minutes of operation. Considering that in an actual experiment we can tolerate a few um erosion, this experiment shows that the capillary operating under conditions for which good guiding was observed could last more than 20 hours. Future tests may prove significantly longer operation.

IV. CONCLUSION

In order to increase the repetition rate of capillary discharge waveguides, erosion due to discharge heating in a capillary discharge waveguide was mitigated by appropriate choice of current pulse amplitude and width. High laser energy transmission and small output laser modes showed that peak current as low as 50 A is suitable for waveguide formation for capillary radius 125 μm, density $\approx 10^{18}\,\mathrm{cm}^{-3}$, and pulse FWHM 160 ns. Surface profile measurements for peak current 80 A showed no observable sapphire erosion taking place.

Thermal simulations showed a repetition rate limit of tens of kHz for the case described above using room temperature cooling, and fluid simulations showed that kHz operation was possible with the current design. Modifications to the gas feed geometry or capillary length could improve upon this. Experiments showed that the flow of gas through the capillary had to be increased to keep the plasma emission (and hence density) constant when increasing the repetition rate from 1 Hz to 1 kHz, which was consistent with a moderate rise in temperature of the sapphire walls and hydrogen gas. Stable operation of the capillary could be achieved at 1 kHz repetition rate once time was allowed for temperature stabilization, resulting in a factor 2 improvement on the standard deviation of light emitted from the plasma and current through the waveguide. Ten million discharges were fired without observable erosion of the sapphire wall, which enables applications such as electron beam focusing to kHz repetition rates.

For use in LPAs ablation of the wall material should be avoided by employing a sufficiently high quality laser mode. In addition, the heat load due to residual wake energy must also be considered and future work should investigate efficient removal of the waste energy via photon acceleration of a trailing pulse[43]. Although in theory all of the wake energy could be removed using a trailing pulse in the linear regime of an LPA, practical considerations such as laser evolution may require the waveguide to withstand increased heat deposition. In this case a capillary material capable of surviving increased heat load is desirable, and simulation showed that the maximum heat load that can be dissipated by diamond is two orders of magnitude higher than for sapphire.

ACKNOWLEDGMENTS

We appreciate useful discussions with H. Mao, C. Geddes, N. Matlis, and C. Schroeder and technical contributions from D. Syversrud, G. Mannino, N. Ybarolazza and D. Evans. This work was supported by the Director, Office of Science, Office of High Energy Physics, of the U.S. Department of Energy under Contract No. DE-SC0008421 and DE-AC02-05CH11231.

[1] E. Esarey, C. B. Schroeder, and W. P. Leemans, Rev. Mod. Phys. **81**, 1229 (2009).

[2] W. P. Leemans, B. Nagler, A. J. Gonsalves, C. Tóth, K. Nakamura, C. G. R. Geddes, E. Esarey, C. B. Schroeder, and S. M. Hooker, Nature Physics **2**, 696 (2006), 1745-2473 10.1038/nphys418 10.1038/nphys418.

[3] C. E. Clayton, J. E. Ralph, F. Albert, R. A. Fonseca, S. H. Glenzer, C. Joshi, W. Lu, K. A. Marsh, S. F. Martins, W. B. Mori, A. Pak, F. S. Tsung, B. B. Pollock, J. S. Ross, L. O. Silva, and D. H. Froula, Phys. Rev. Lett. **105**, 105003 (2010).

[4] X. Wang, R. Zgadzaj, N. Fazel, Z. Li, S. A. Yi, X. Zhang, W. Henderson, Y.-Y. Chang, R. Korzekwa, H.-E. Tsai, C.-H. Pai, H. Quevedo, G. Dyer, E. Gaul, M. Martinez, A. C. Bernstein, T. Borger, M. Spinks, M. Donovan, V. Khudik, G. Shvets, T. Ditmire, and M. C. Downer, Nature Communications **4**, 1988 (2013).

[5] H. T. Kim, K. H. Pae, H. J. Cha, I. J. Kim, T. J. Yu, J. H. Sung, S. K. Lee, T. M. Jeong, and J. Lee, Phys. Rev. Lett. **111**, 165002 (2013).

[6] W. P. Leemans, A. Gonsalves, H. S. Mao, K. Nakamura, C. Benedetti, C. B. Schroeder, Cs. Tóth, J. Daniels, D. E. Mittelberger, S. S. Bulanov, J.-L. Vay, C. G. R. Geddes, and E. Esarey, Phys. Rev. Lett. **113**, 245002 (2014).

[7] A. J. Gonsalves, K. Nakamura, J. Daniels, H.-S. Mao, C. Benedetti, C. B. Schroeder, C. Tóth, J. van Tilborg, D. E. Mittelberger, S. S. Bulanov, J.-L. Vay, C. G. R. Geddes, E. Esarey, and W. P. Leemans, Physics of Plasmas **22**, 056703 (2015).

[8] F. Grüner, S. Becker, U. Schramm, M. Fuchs, R. Weingartner, D. Habs, J. Meyer-ter Vehn, M. Geissler, M. Ferrario, L. Serafini,

B. van der Geer, H. Backe, W. Lauth, and S. Reiche, Applied Physics B-Lasers and Optics **86**, 431 (2007).
[9]S. Cipiccia, M. R. Islam, B. Ersfeld, R. P. Shanks, E. Brunetti, G. Vieux, X. Yang, R. C. Issac, S. M. Wiggins, G. H. Welsh, M.-P. Anania, D. Maneuski, R. Montgomery, G. Smith, M. Hoek, D. J. Hamilton, N. R. C. Lemos, D. Symes, P. P. Rajeev, V. O. Shea, J. M. Dias, and D. A. Jaroszynski, Nature Phys. **7**, 867 (2011).
[10]W. P. Leemans, C. G. R. Geddes, J. Faure, C. Tóth, J. van Tilborg, C. B. Schroeder, E. Esarey, G. Fubiani, D. Auerbach, B. Marcelis, M. A. Carnahan, R. A. Kaindl, J. Byrd, and M. C. Martin, Phys. Rev. Lett. **91**, 074802 (2003).
[11]A. R. Maier, A. Meseck, S. Reiche, C. B. Schroeder, T. Seggebrock, and F. Grüner, Phys. Rev. X **2**, 031019 (2012).
[12]P. Tomassini, A. Bacci, J. Cary, M. Ferrario, A. Giulietti, D. Giulietti, L. Gizzi, L. Labate, L. Serafini, V. Petrillo, and C. Vaccarezza, Plasma Science, IEEE Transactions on **36**, 1782 (2008).
[13]Z. Huang, Y. Ding, and C. B. Schroeder, Phys. Rev. Lett. **109**, 204801 (2012).
[14]W. Leemans and E. Esarey, Phys. Today **62**, 44 (2009).
[15]C. B. Schroeder, E. Esarey, C. G. R. Geddes, C. Benedetti, and W. P. Leemans, Phys. Rev. ST Accel. Beams **13**, 101301 (2010).
[16]C. G. Geddes, S. Rykovanov, N. H. Matlis, S. Steinke, J.-L. Vay, E. H. Esarey, B. Ludewigt, K. Nakamura, B. J. Quiter, C. B. Schroeder, C. Toth, and W. P. Leemans, Nuclear Instruments and Methods in Physics Research Section B: Beam Interactions with Materials and Atoms **350**, 116 (2015).
[17]G. Mourou, B. Brocklesby, T. Tajima, and J. Limpert, Nat Photon **7**, 258 (2013).
[18]T. P. A. Ibbotson, N. Bourgeois, T. P. Rowlands-Rees, L. S. Caballero, S. I. Bajlekov, P. A. Walker, S. Kneip, S. P. D. Mangles, S. R. Nagel, C. A. J. Palmer, N. Delerue, G. Doucas, D. Urner, O. Chekhlov, R. J. Clarke, E. Divall, K. Ertel, P. S. Foster, S. J. Hawkes, C. J. Hooker, B. Parry, P. P. Rajeev, M. J. V. Streeter, and S. M. Hooker, Phys. Rev. ST Accel. Beams **13**, 031301 (2010).
[19]A. Butler, D. J. Spence, and S. M. Hooker, Phys. Rev. Lett. **89**, 185003 (2002).
[20]N. A. Bobrova, A. A. Esaulov, J. Sakai, P. V. Sasorov, D. J. Spence, A. Butler, S. M. Hooker, and S. V. Bulanov, Phys. Rev. E **65**, 016407 (2002).
[21]J. van Tilborg, S. Steinke, C. G. R. Geddes, N. H. Matlis, B. H. Shaw, A. J. Gonsalves, J. V. Huijts, K. Nakamura, J. Daniels, C. B. Schroeder, E. Esarey, S. S. Bulanov, N. A. Bobrova, P. V. Sasorov, and W. P. Leemans, Physical Review Letters **115** (2015), 10.1103/PhysRevLett.115.184802.
[22]S. Steinke, J. van Tilborg, C. Benedetti, C. G. R. Geddes, C. B. Schroeder, J. Daniels, K. K. Swanson, A. J. Gonsalves, K. Nakamura, B. H. Shaw, E. Esarey, and W. P. Leemans, submitted to Nature (2015).
[23]D. M. Gaudiosi, B. Reagan, T. Popmintchev, M. Grisham, M. Berrill, O. Cohen, B. C. Walker, M. M. Murnane, H. C. Kapteyn, and J. J. Rocca, Phys. Rev. Lett. **96**, 203001 (2006).
[24]A. Butler, A. J. Gonsalves, C. M. McKenna, D. J. Spence, S. M. Hooker, S. Sebban, T. Mocek, I. Bettaibi, and B. Cros, Phys. Rev. Lett. **91**, 205001 (2003).
[25]A. Zigler, Y. Ehrlich, C. Cohen, J. Krall, and P. Sprangle, Journal of the Optical Society of America B-Optical Physics **13**, 68 (1996).
[26]Y. Ehrlich, C. Cohen, A. Zigler, J. Krall, P. Sprangle, and E. Esarey, Physical Review Letters **77**, 4186 (1996).
[27]T. Hosokai, M. Kando, H. Dewa, H. Kotaki, S. Kondo, N. Hasegawa, K. Nakajima, and K. Horioka, Optics Letters **25**, 10 (2000).
[28]A. J. Gonsalves, *Investigation of a Hydrogen-filled Capillary Discharge Waveguide for Laser-driven Plasma Accelerators*, Thesis, University of Oxford (2006).
[29]P. Sprangle, E. Esarey, J. Krall, and G. Joyce, Physical review letters **69**, 2200 (1992).
[30]S. I. Braginskii, Sov. Phys. JETP **6**, 283 (1958).
[31]S. Braginskii, Reviews of Plasma Physics **1**, 205 (1963).
[32]N. Bobrova and P. Sasorov, Plasma Physics Reports **19**, 409 (1993).
[33]N. A. Bobrova, E. Lazzaro, and P. V. Sasorov, Physics of Plasmas **12**, 022105 (2005).
[34]S. I. Braginskii, JETP **33**, 645 (1957).
[35]R. Pease, Proceedings of the Physical Society. Section B **70**, 11 (1957).
[36]W. P. Leemans, C. E. Clayton, W. B. Mori, K. A. Marsh, P. K. Kaw, A. Dyson, C. Joshi, and J. M. Wallace, Phys. Rev. A **46**, 1091 (1992).
[37]D. J. Spence and S. M. Hooker, Phys. Rev. E **63**, 015401 (2000).
[38]A. J. Gonsalves, T. P. Rowlands-Rees, B. H. P. Broks, J. J. A. M. van der Mullen, and S. M. Hooker, Phys. Rev. Lett. **98**, 025002 (2007).
[39]D. Jaroszynski, R. Bingham, E. Brunetti, B. Ersfeld, J. Gallacher, B. van Der Geer, R. Issac, S. Jamison, D. Jones, M. De Loos, *et al.*, Philosophical Transactions of the Royal Society A: Mathematical, Physical and Engineering Sciences **364**, 689 (2006).
[40]"Ansys® academic research, release 14.5,".
[41]W. L. Waldron, A. J. Gonsalves, and W. P. Leemans, in *Power Modulator and High Voltage Conference (IPMHVC), 2014 IEEE International* (2014) p. 57.
[42]F. M. Sharipov and V. D. Seleznev, Journal of Vacuum Science and Technology A **12**, 2933 (1994).
[43]C. B. C. B. Schroeder, E. Esarey and W. P. Leemans, in *Proc. of 2014 Advanced Accelerator Concepts Workshop (in press)* (2015).

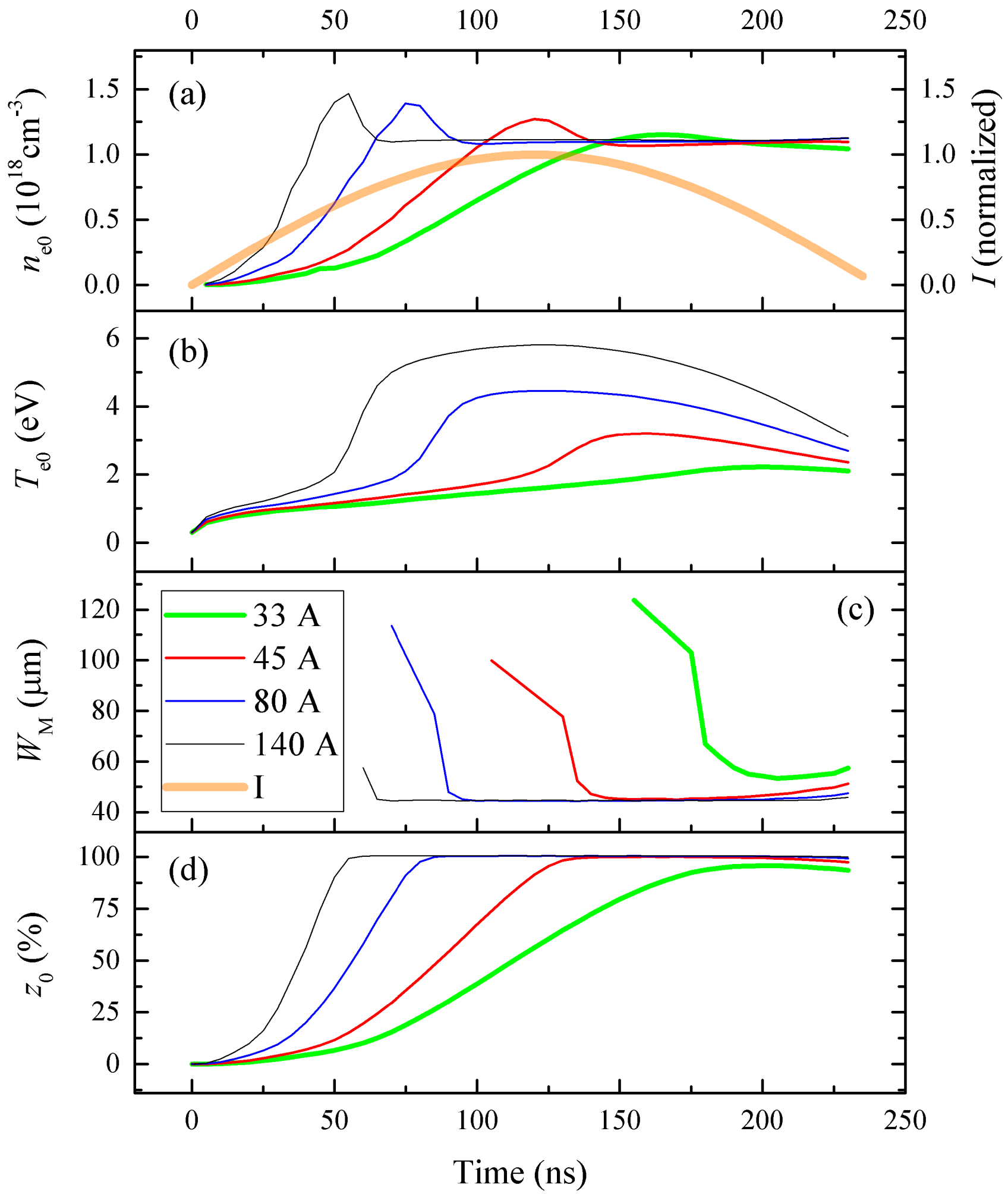
(a)
(b)
(c)
(d)
n_{e0} (10^{18}cm^{-3})
I (normalized)
T_{e0} (eV)
W_M (μm)
z_0 (%)
33 A
45 A
80 A
140 A
I
Time (ns)

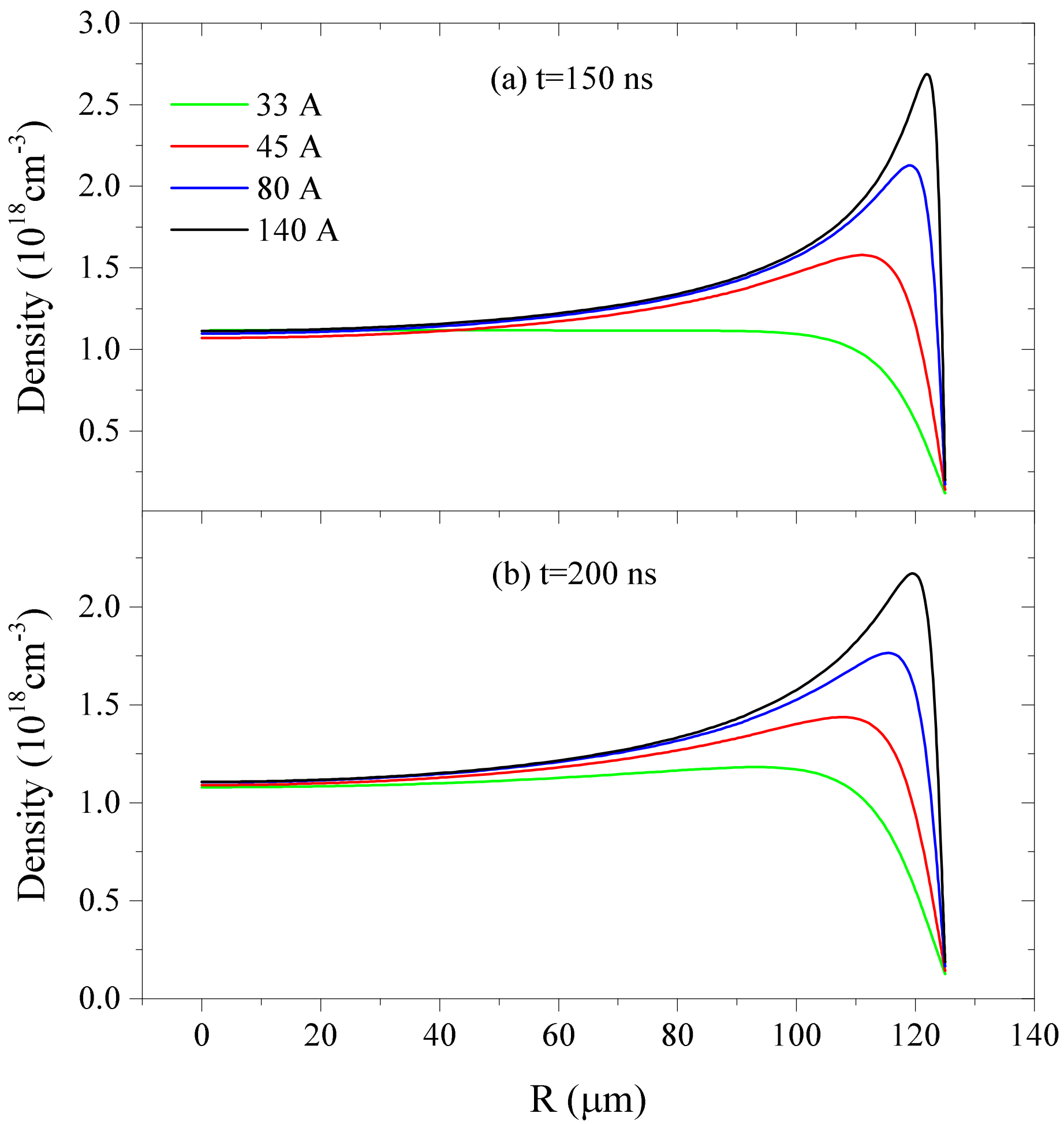
(a) t=150 ns
33 A
45 A
80 A
140 A
Density (10^{18}cm^{-3})
3.0
2.5
2.0
1.5
1.0
0.5
(b) t=200 ns
Density (10^{18}cm^{-3})
2.0
1.5
1.0
0.5
0.0
0
20
40
60
80
100
120
140
R (μm)

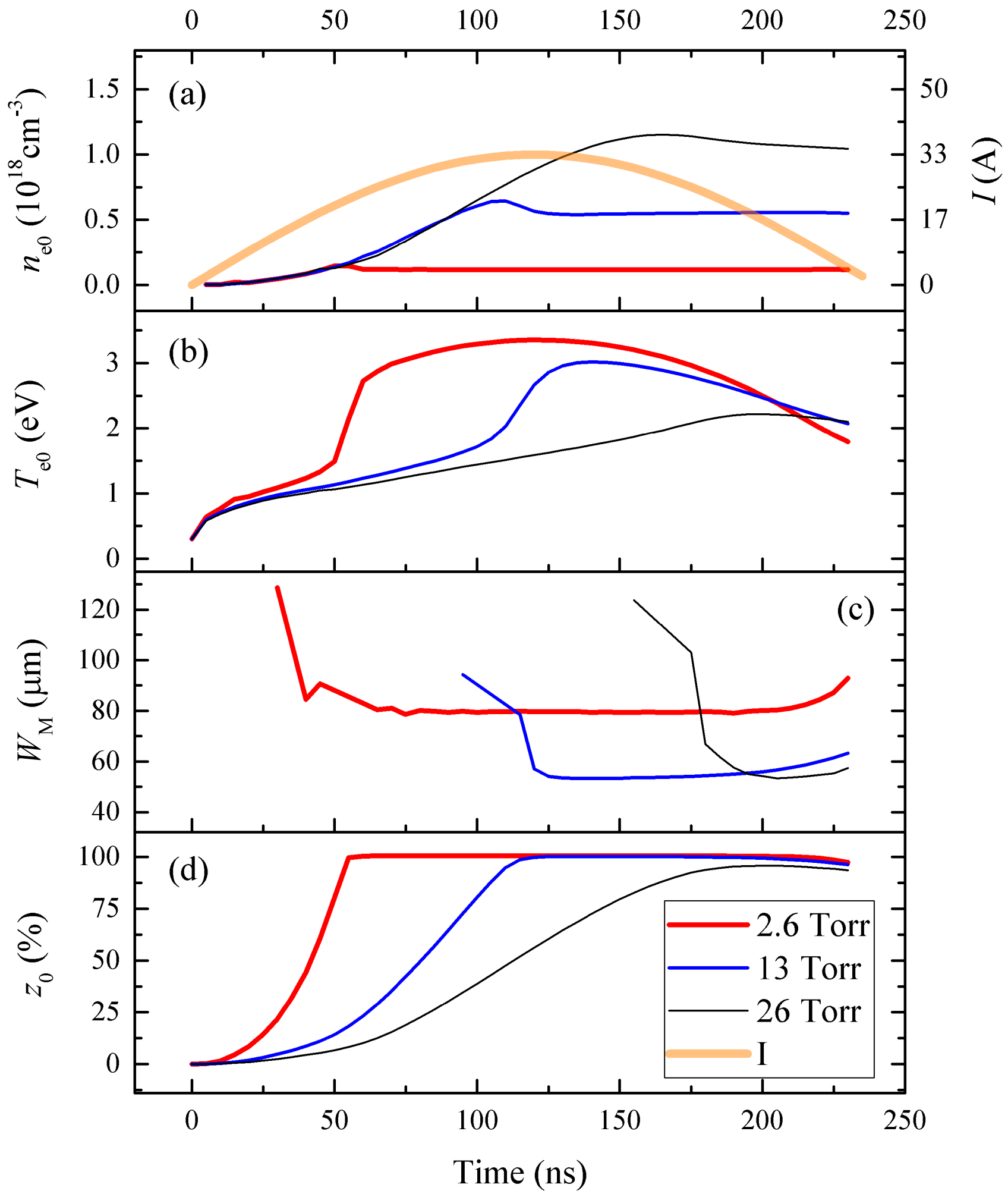
(a)
(b)
(c)
(d)
n_{e0} (10^{18}cm^{-3})
T_{e0} (eV)
W_M (μm)
z_0 (%)
I (A)
Time (ns)
2.6 Torr
13 Torr
26 Torr
I

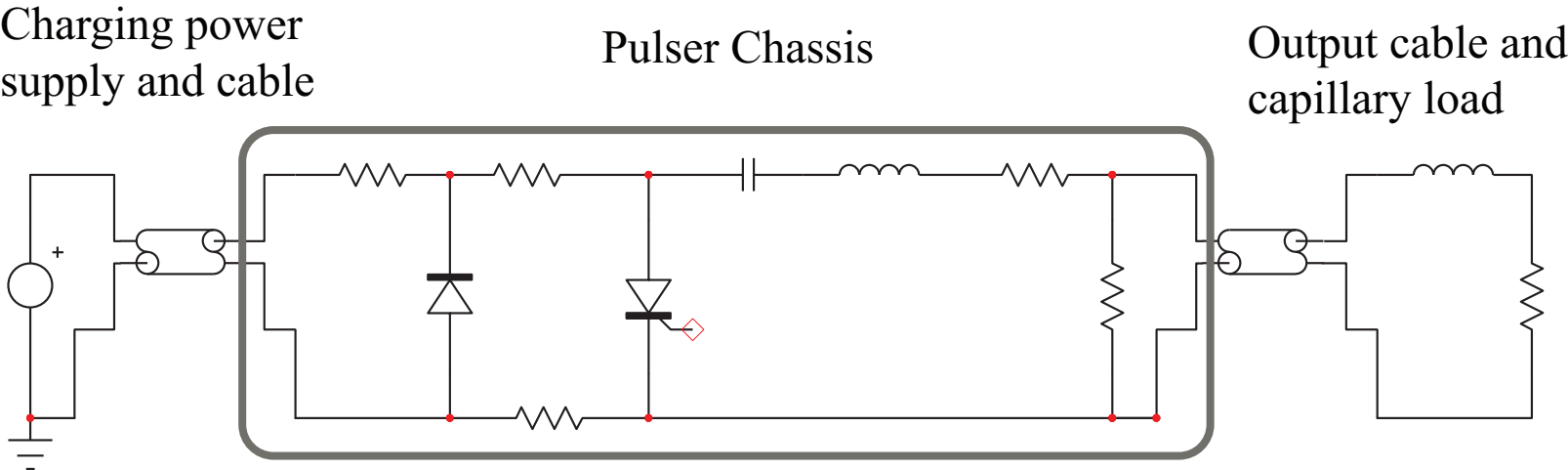
Charging power supply and cable
Pulser Chassis
Output cable and capillary load
+
-

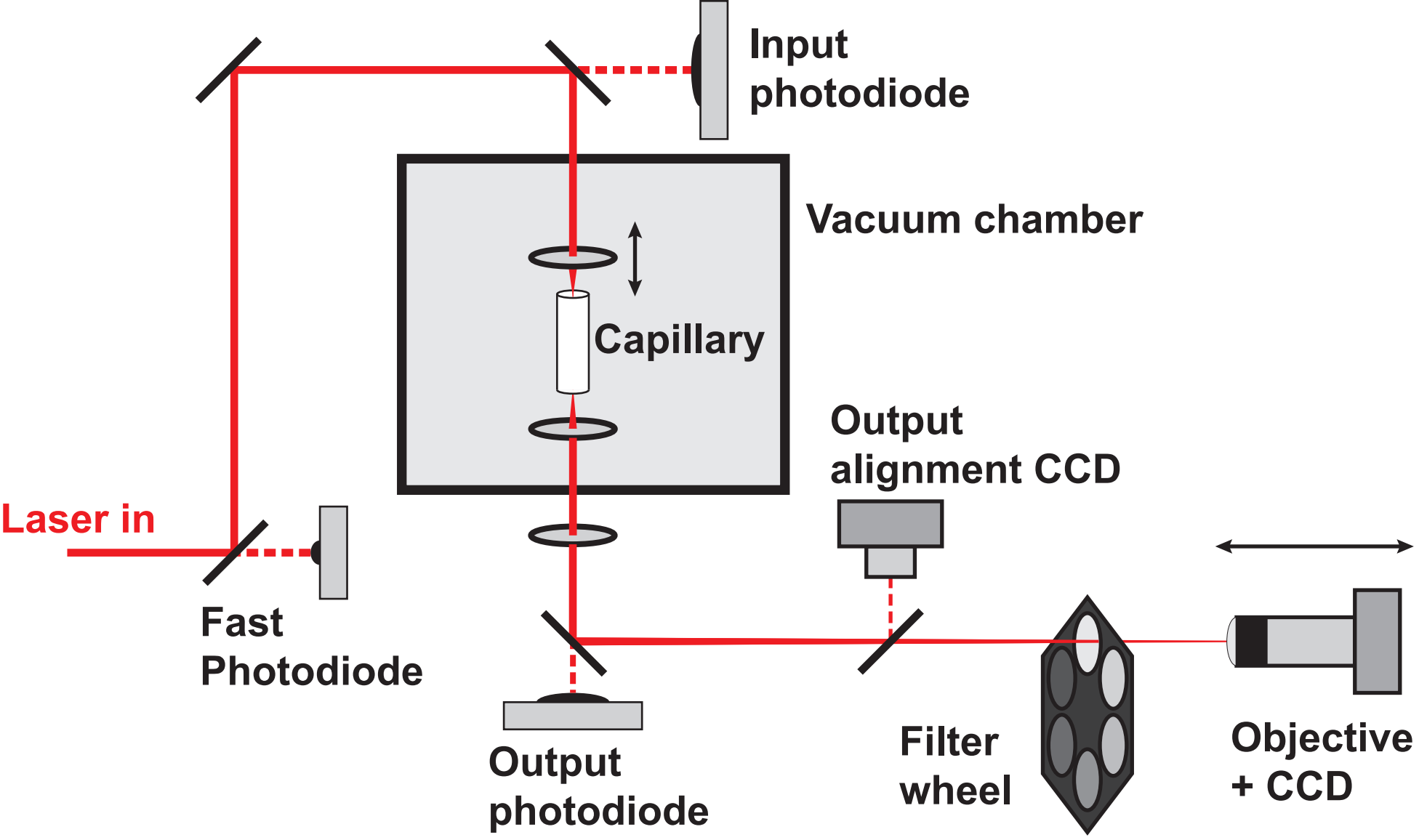
Input
photodiode
Vacuum chamber
Capillary
Output
alignment CCD
Laser in
Fast
Photodiode
Output
photodiode
Filter
wheel
Objective
+ CCD

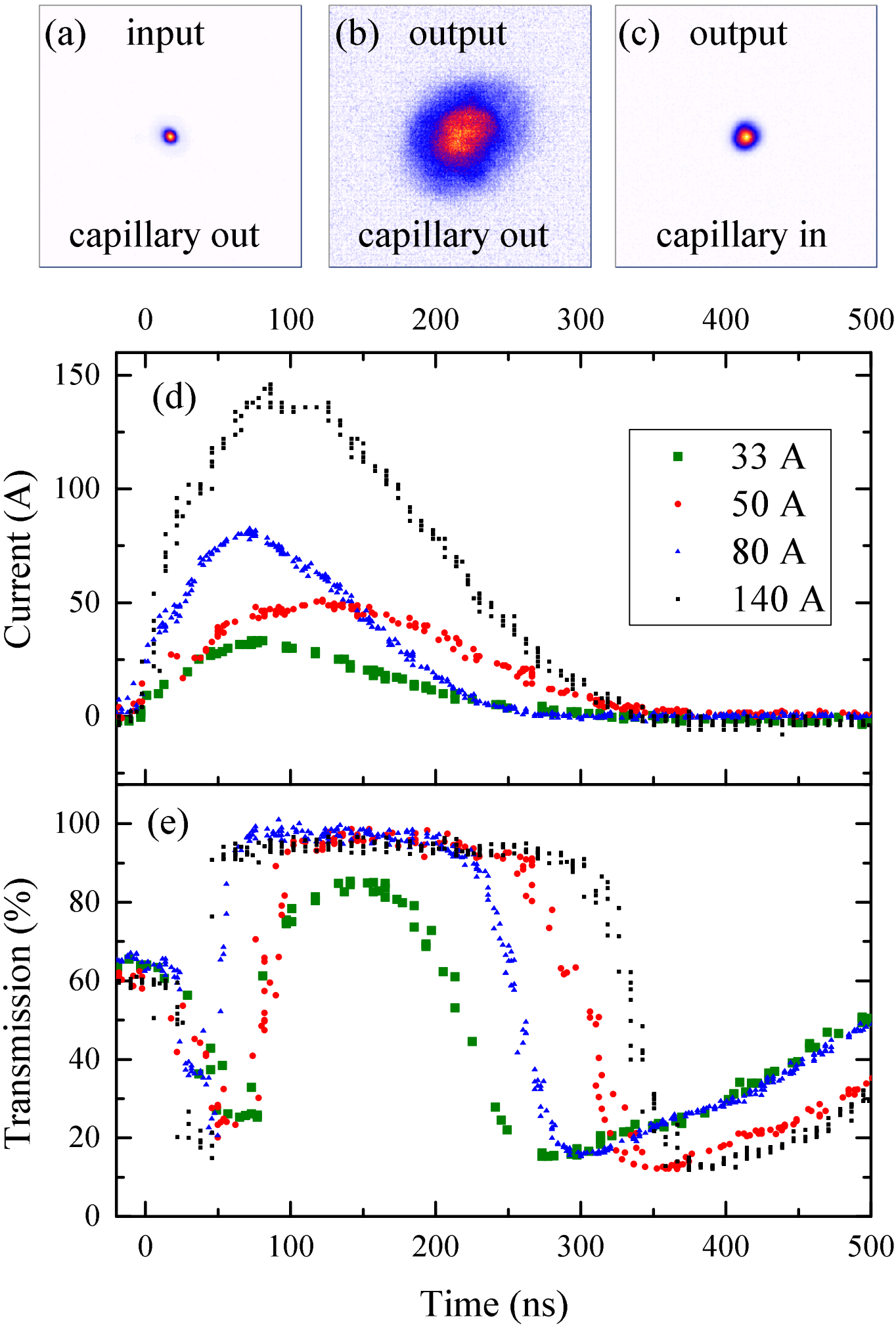
(a) input
capillary out
(b) output
capillary out
(c) output
capillary in
(d)
(e)
33 A
50 A
80 A
140 A
Current (A)
Transmission (%)
Time (ns)
0
100
200
300
400
500
150
50
20
60
40
80

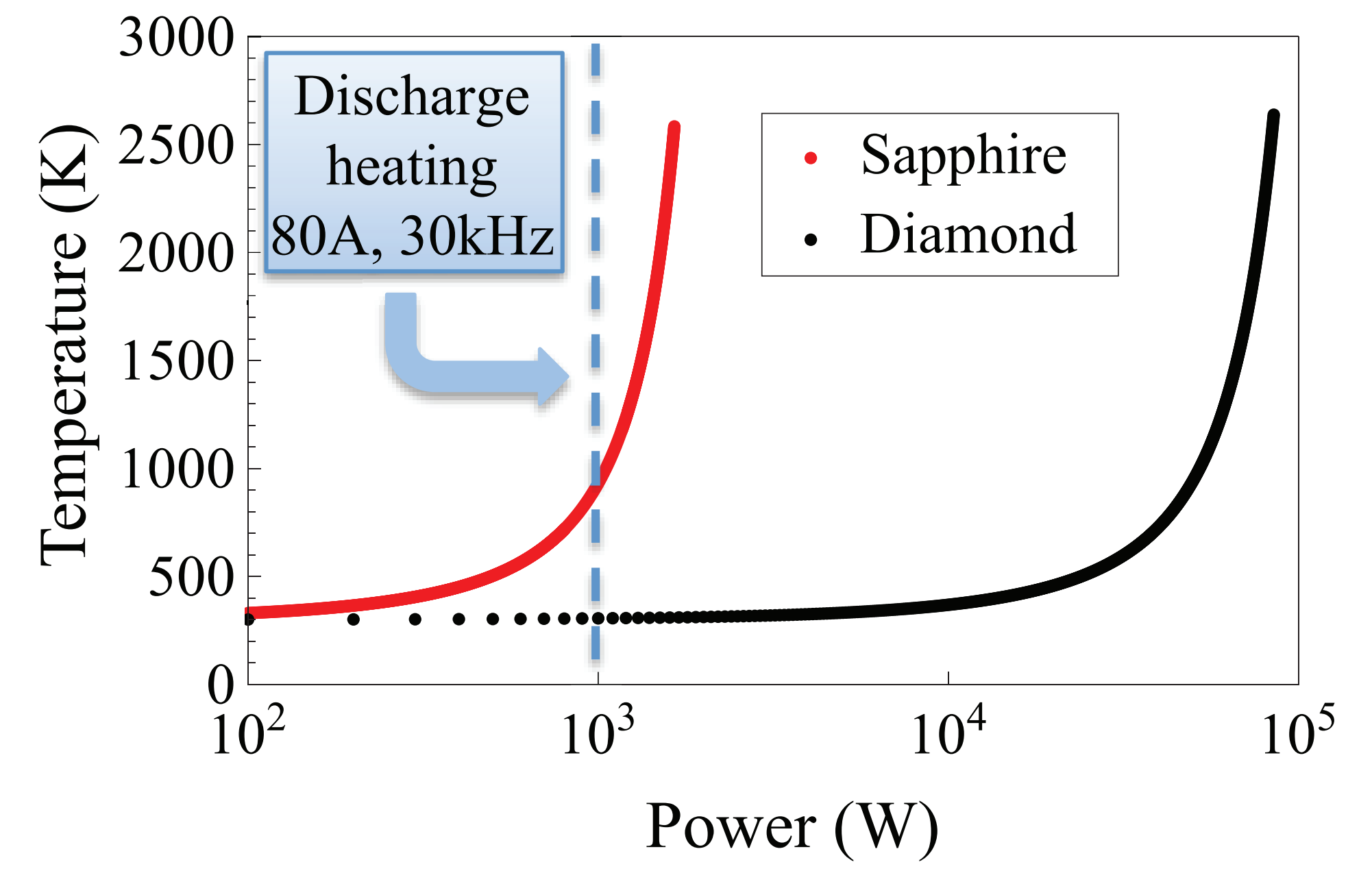
Discharge
heating
80A, 30kHz
Sapphire
Diamond
Temperature (K)
3000
2500
2000
1500
1000
500
0
10^2
10^3
10^4
10^5
Power (W)

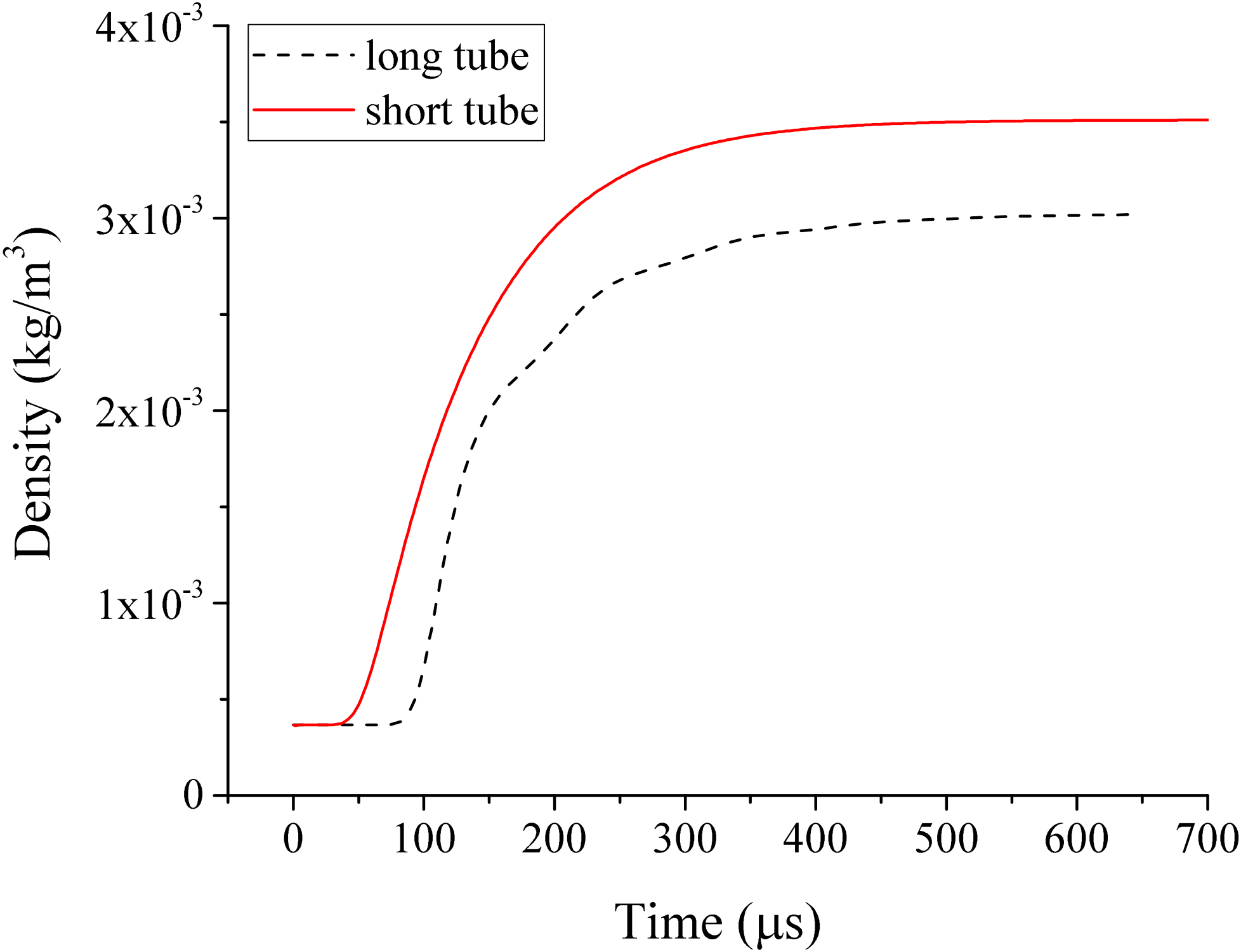
long tube
short tube
4x10-3
3x10-3
2x10-3
1x10-3
0
Density (kg/m3)
0
100
200
300
400
500
600
700
Time (μs)

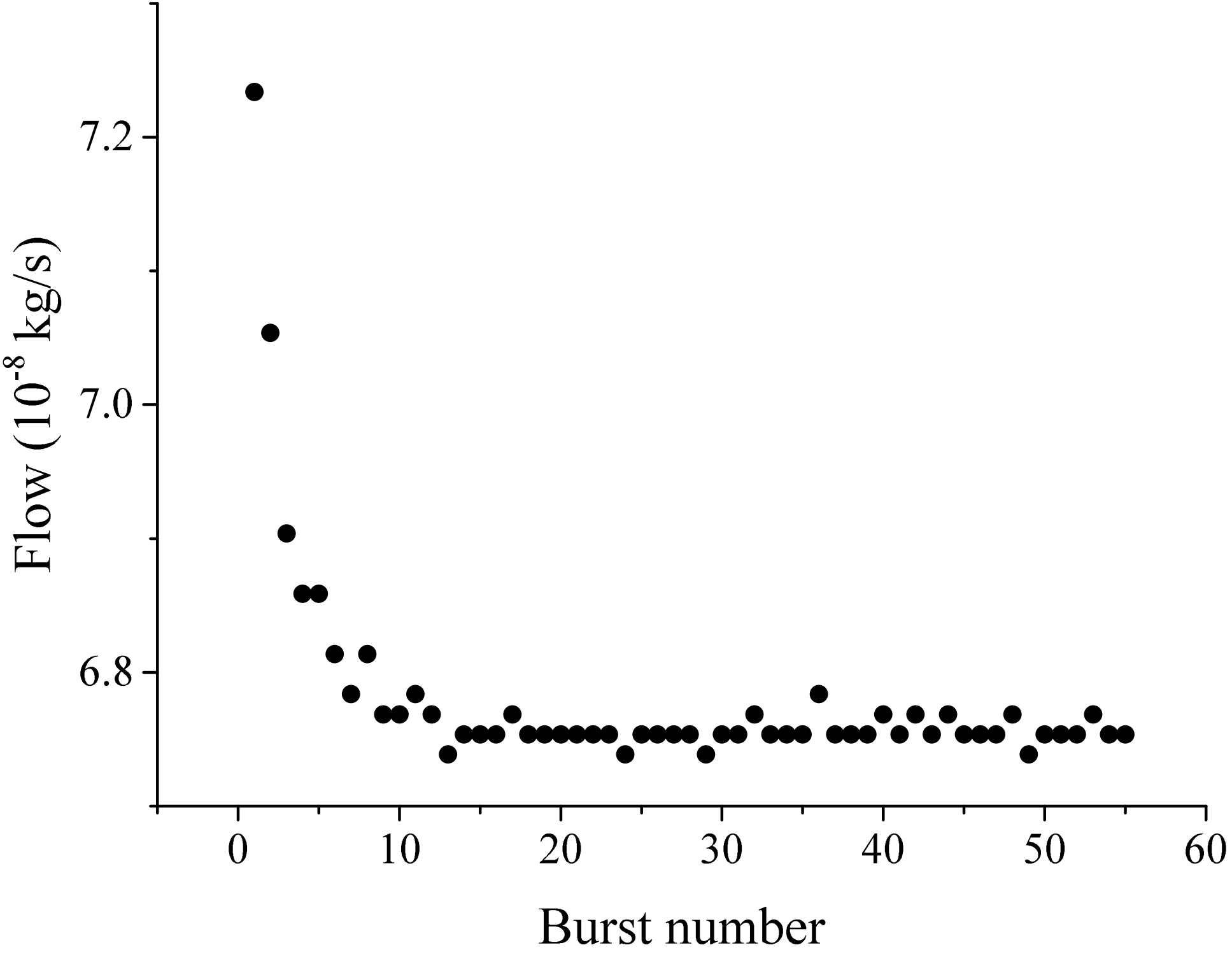
7.2
7.0
6.8
Flow (10^{-8} kg/s)
0
10
20
30
40
50
60
Burst number

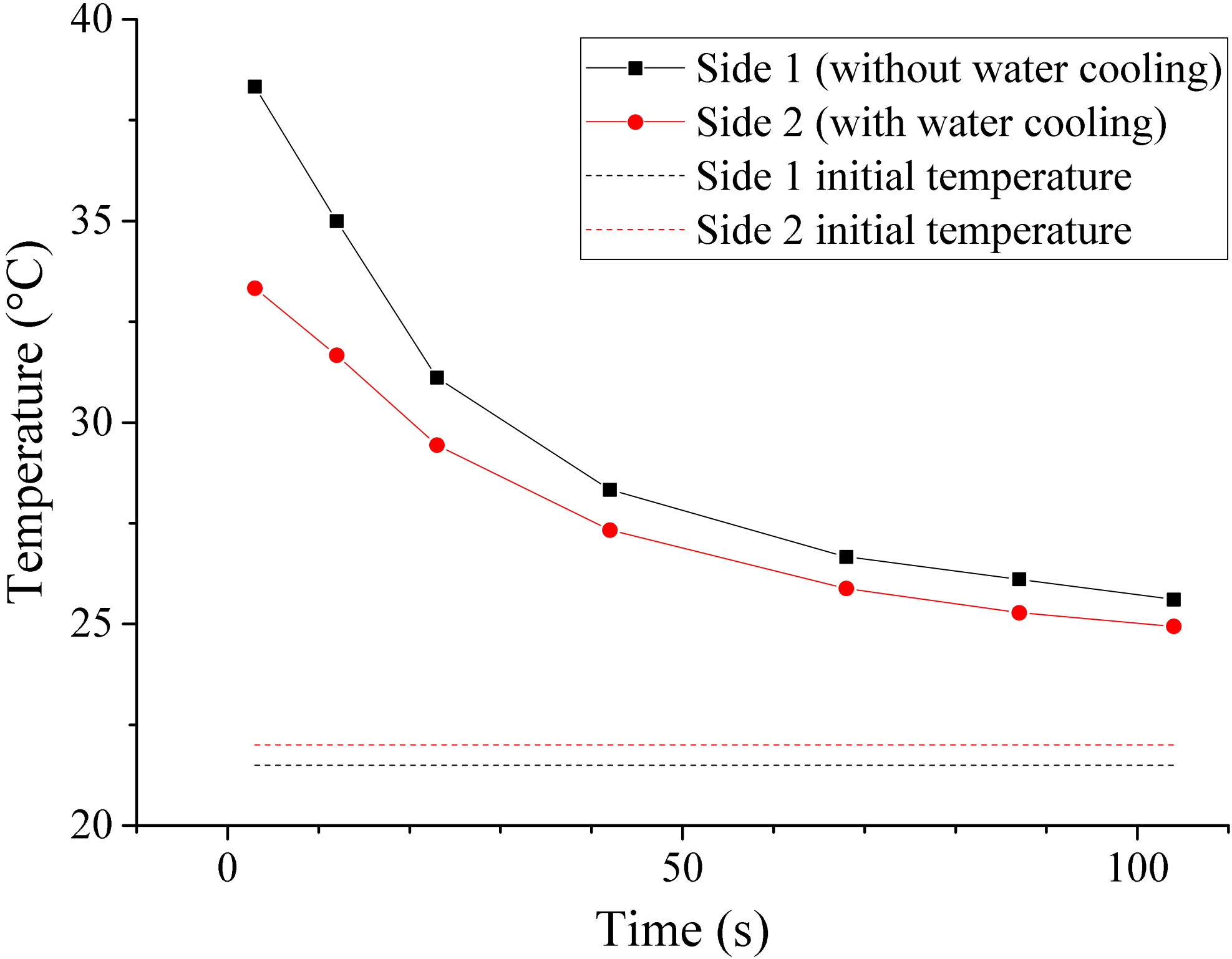
Side 1 (without water cooling)
Side 2 (with water cooling)
Side 1 initial temperature
Side 2 initial temperature
Temperature (°C)
Time (s)
40
35
30
25
20
0
50
100

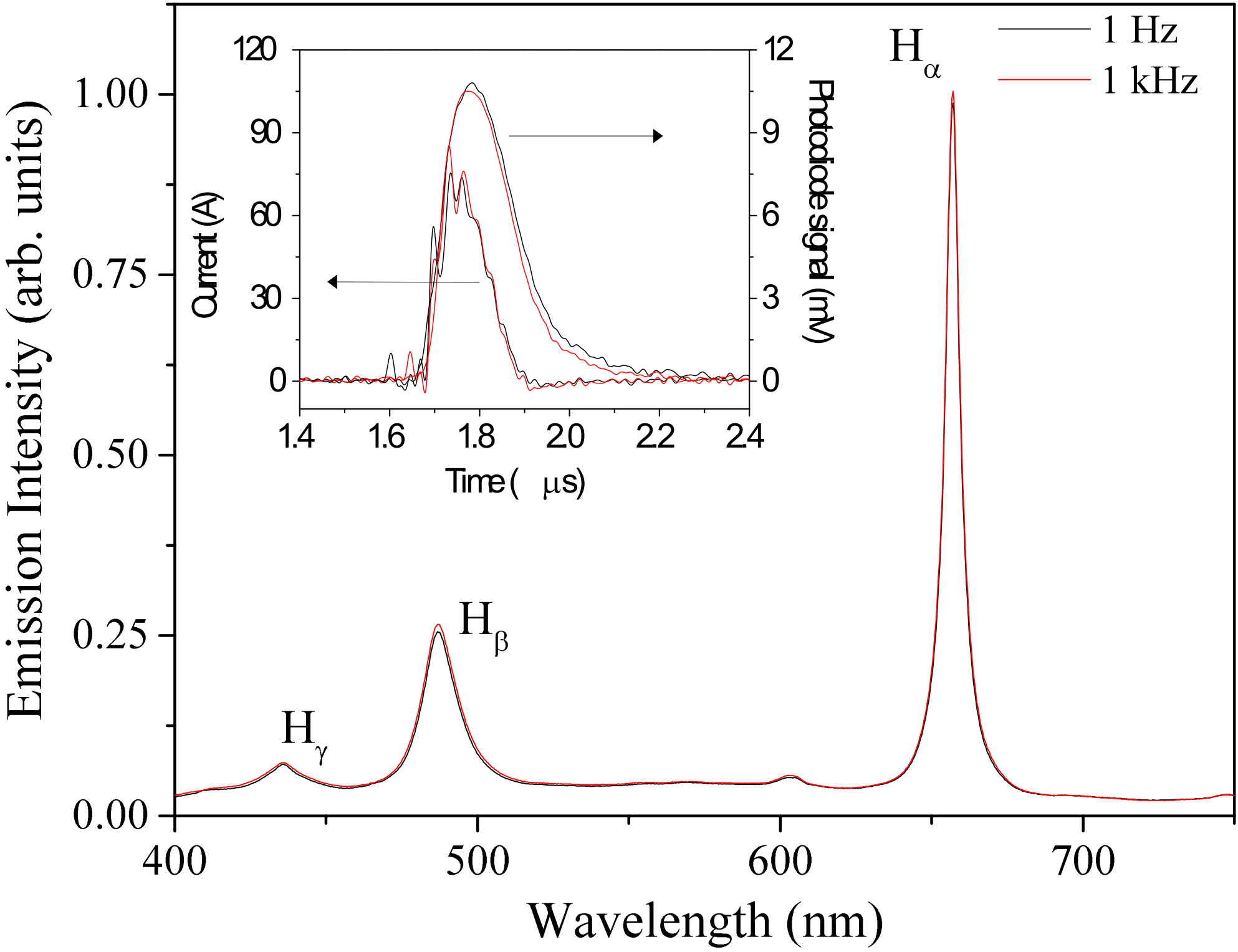
1 Hz
1 kHz
H_α
H_β
H_γ
Emission Intensity (arb. units)
Wavelength (nm)
1.00
0.75
0.50
0.25
0.00
400
500
600
700
Current (A)
Photodiode signal (mV)
Time (μs)
120
90
60
30
0
12
9
6
3
0
1.4
1.6
1.8
20
22
24

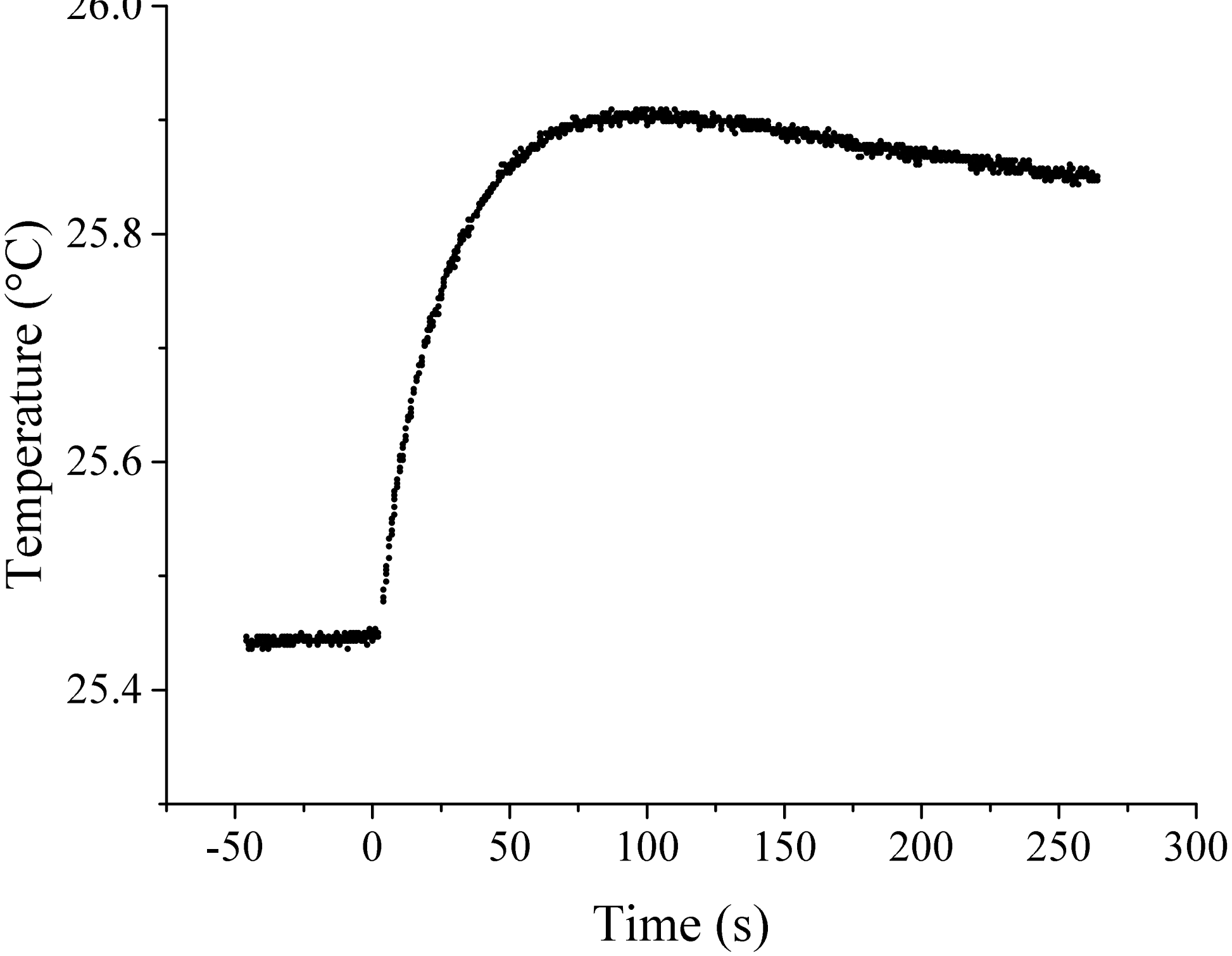
26.0
25.8
25.6
25.4
Temperature (°C)
-50
0
50
100
150
200
250
300
Time (s)

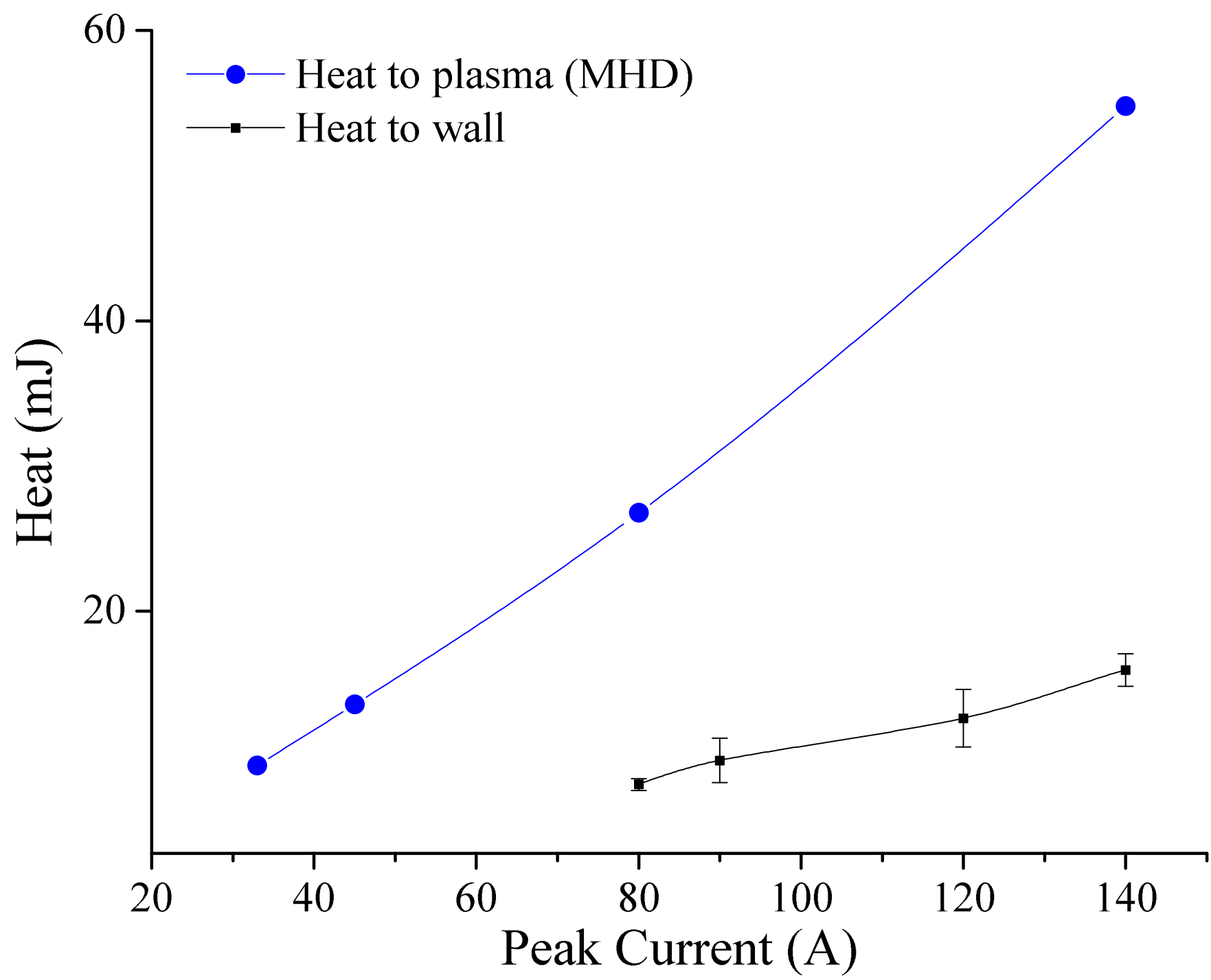
Heat to plasma (MHD)
Heat to wall
Heat (mJ)
Peak Current (A)
60
40
20
20
40
60
80
100
120
140

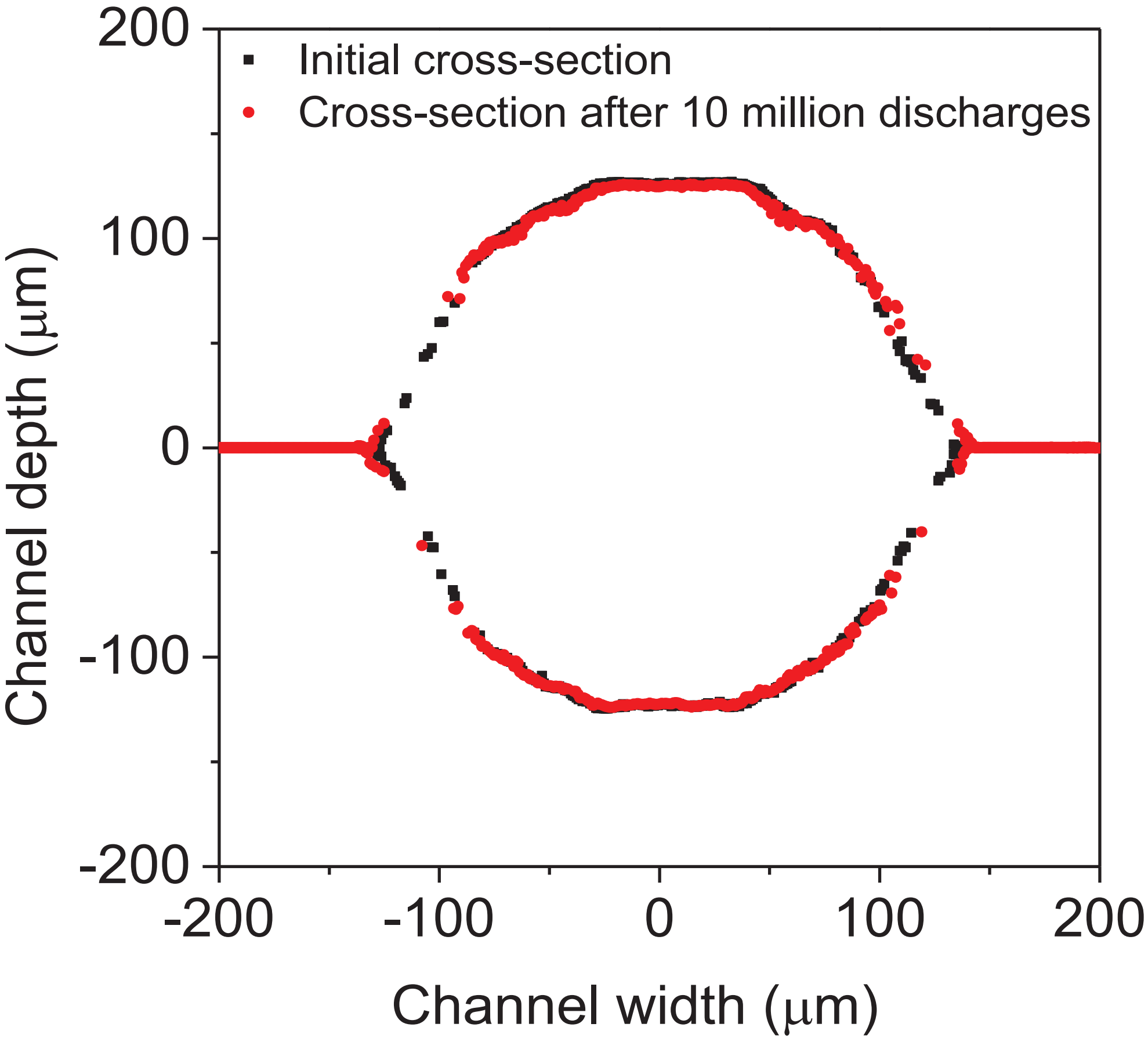
Initial cross-section
Cross-section after 10 million discharges
Channel depth (μm)
Channel width (μm)
200
100
0
-100
-200
-200
-100
0
100
200

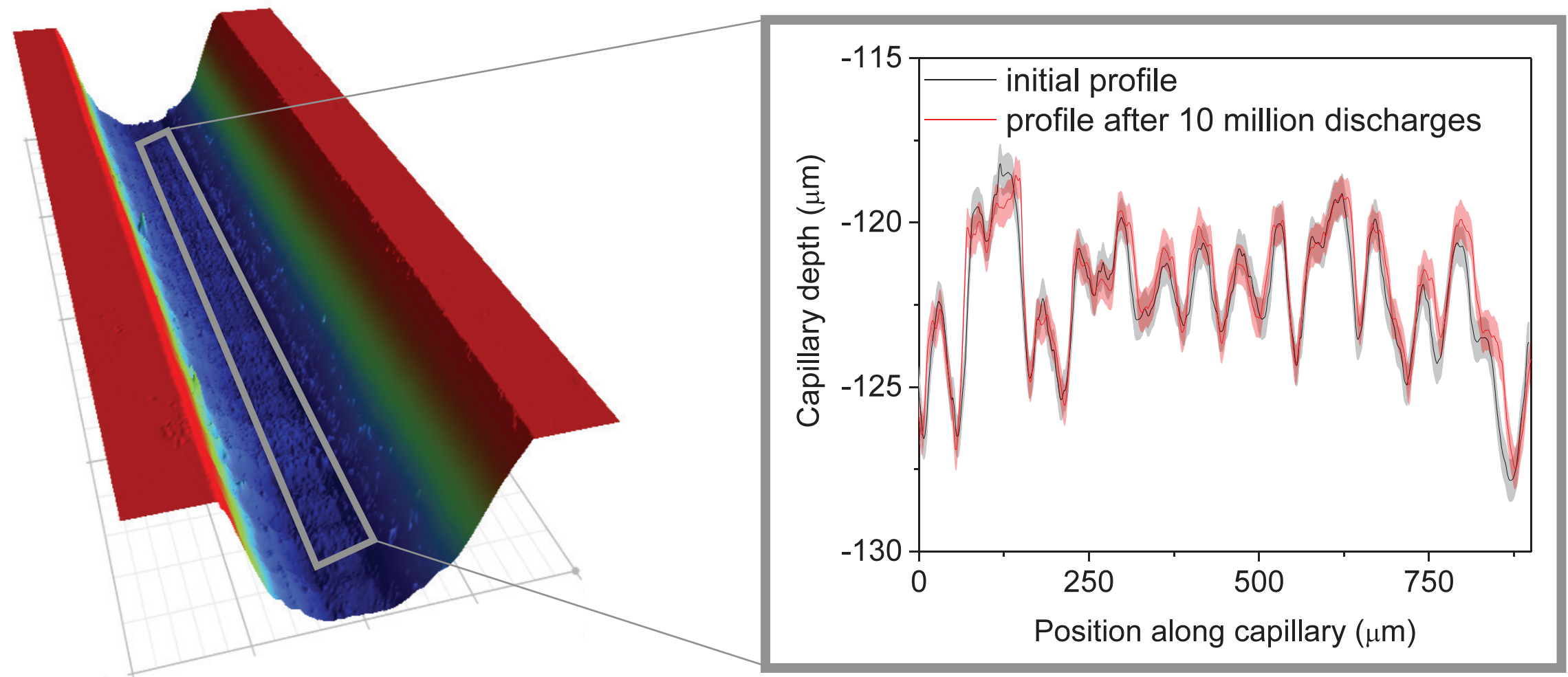
initial profile
profile after 10 million discharges
Capillary depth (μm)
-115
-120
-125
-130
0
250
500
750
Position along capillary (μm)